UNIVERSITY OF CALIFORNIA SAN DIEGO

Temporal laser pulse shape optimization for EUV lithography with FLASH and SPECT3D simulations

A Thesis submitted in partial satisfaction of the requirements of the requirements for the degree Master of Science

in

Engineering Sciences (Mechanical Engineering)

by

Brian Lee

Committee in Charge:

Professor Farhat Beg, Chair

Professor Robert Bitmead

Professor Renkun Chen

2021

The Thesis of Brian Lee is approved, and it is acceptable in quality and form for publication on microfilm and electronically.

University of California San Diego

2021

DEDICATION

I dedicate this thesis to my family, separated by the pandemic: to my mother, to whom I owe my resilience, discipline and work ethic; to my father, to whom I owe my humor, moral center, and critical understanding of the world; and to my sisters, to whom I owe more of my time, attention and love.

TABLE OF CONTENTS

LIST OF FIGURES

LIST OF TABLES

ACKNOWLEDGEMENTS

I would like to acknowledge Professor Farhat Beg, my thesis advisor, chair of my committee, and a huge reason for my graduate school application a-year-and-a-half ago. Without his encouragement, guidance and support, I would not have completed this thesis.

I would also like to acknowledge Kazuki Matsuo and Mathieu Bailly-Grandvaux, two of my collaborators at the High Energy Density Physics (HEDP) Group. With their orientation, teaching, and constructive criticism, I have learned and accomplished way more than I would have alone.

Chapter 3, in part, is currently being prepared for submission for publication of the material. Lee, Brian; Matsuo, Kazuki; Bailly-Grandvaux, Mathieu; Beg, Farhat. The thesis author was the primary investigator and author of this material.

Chapter 4, in part, is currently being prepared for submission for publication of the material. Lee, Brian; Matsuo, Kazuki; Bailly-Grandvaux, Mathieu; Beg, Farhat. The thesis author was the primary investigator and author of this material.

ABSTRACT OF THE THESIS

Temporal laser pulse shape optimization for EUV lithography with FLASH and SPECT3D simulations

by

Brian Lee

Master of Science in Engineering Sciences (Mechanical Engineering)

University of California San Diego, 2021

Professor Farhat Beg, Chair

Extreme ultraviolet (EUV) lithography, the etching of fine semiconductor features with EUV light, is based on efficiently generating light of a wavelength within a narrow bandwidth around 13.5 nm by irradiating tin droplets with a laser. Simulating this process is beneficial to aid the target design and optimize the laser-plasma interaction for an enhanced EUV light output. In

this work, we benchmarked the combination of the open source FLASH code and the commercially available SPECT3D against existing experimental data, showing that by stepping down the intensity by approximately a factor of two and shifting the spectra to the right by +0.55 nm, the simulations provide results with a reasonable level of accuracy. Using the benchmarked settings to investigate four novel temporal pulse shapes, we found that the “step down”, “ step up” and “Gaussian ramp” pulses resulted in 1.4%, 4.0%, and 4.0% improvements in conversion efficiency respectively over their energy-equivalent square pulses. With improvements to the atomic level modeling, further benchmarking of the simulations, and the development of a robust open-source community around these two tools, we expect FLASH and SPECT3D to be the tools of choice for new researchers in EUV lithography.

Chapter 1. Introduction to EUV Lithography

1.1 Motivation

In the last two years, extreme ultraviolet (EUV) lithography has become the basis of continued Moore's Law scaling — the empirical observation that transistor count (or, transistor density) doubles every two years. Prior to EUV lithography, many were speculating the imminent death of Moore's Law as a viable expectation for the future of semiconductor scaling, citing heat, size and market limitations as reasons for its demise. [1] In the short-term, much of that pessimism was due to the limitations of the state of the art lithographic system at the time, 193 nm immersion lithography. At its longer wavelength, 193 nm immersion lithography is limited to a 38 nm half pitch, requiring multiple exposures — and, thus, higher costs per wafer — to extend the miniaturization of features. [2] Fortunately, built upon the early work by U.S. National EUV Lithography Program and the EUV LLC [3], ASML has successfully developed and commercialized EUV scanners at the 13.5 nm wavelength, paving the way for smaller transistor features. Now available in commercially in the form of the iPhone 12's A14 Bionic processor [5] and Samsung's DRAM memory [6], chipsets made with EUV lithography are expected to provide further scaling in transistor density, supplying the faster, cheaper and more power-efficient chips needed in an increasingly digitized world.

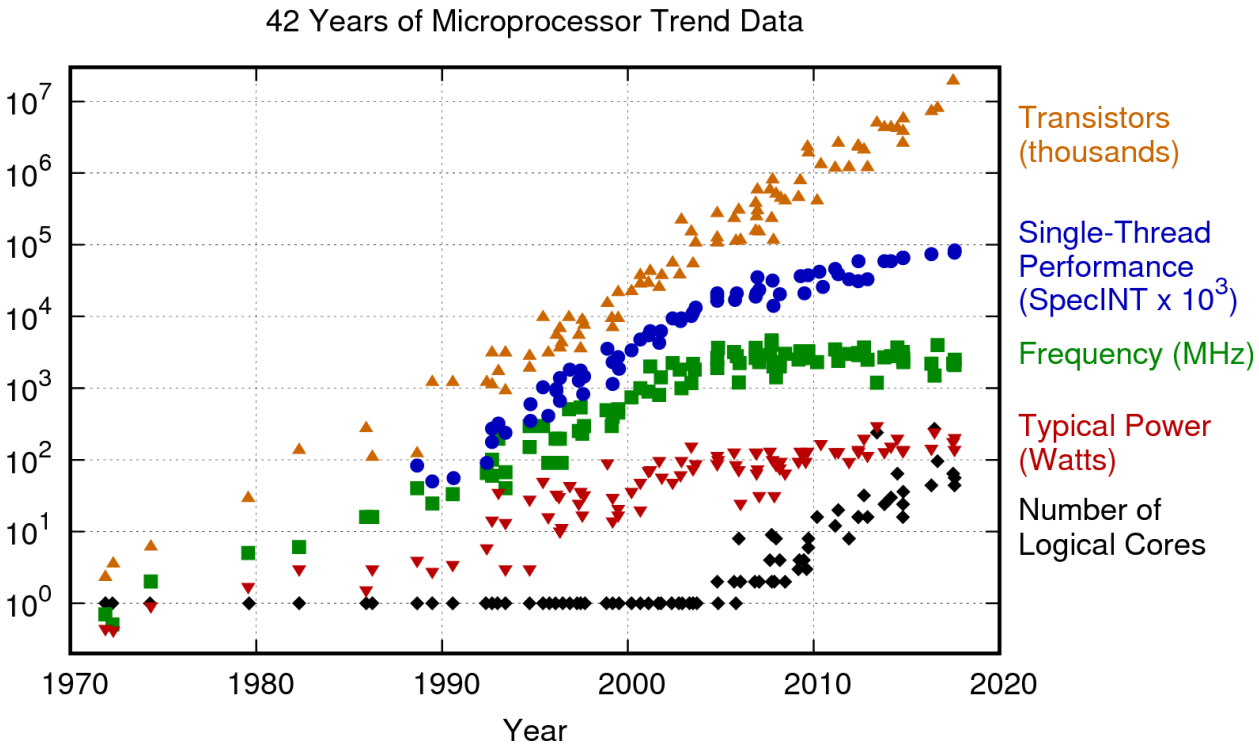

Figure 1.1: Trend of transistor count, single-thread performance, frequency, power and logical core count for 42 years up to 2018. The transistor count plot showing the roughly doubling of transistor count every two years is commonly referred to as Moore's Law. [4]

EUV lithography is designed around the high reflection by Mo/Si multilayer mirrors of light with wavelength of the narrow 2% bandwidth around 13.5 nm — the so-called "in-band" portion of the spectra. [7] This is because any in-band 13.5 nm light created has to be collected, transported, shown through a mask, and reflected onto the wafer by those mirrors. As such, the EUV source, the part of the EUV machine that creates the light needed through tin laser-produced plasma (LPP), is tuned specifically to produce as much of that light as possible. In fact, at the right combination of electron temperature and tin ion density, the spectrum produced shows a sharp peak at around 13.5 nm, producing the light needed relatively efficiently. [8] To measure this, the metric used by industry and researchers alike is conversion efficiency (CE) —

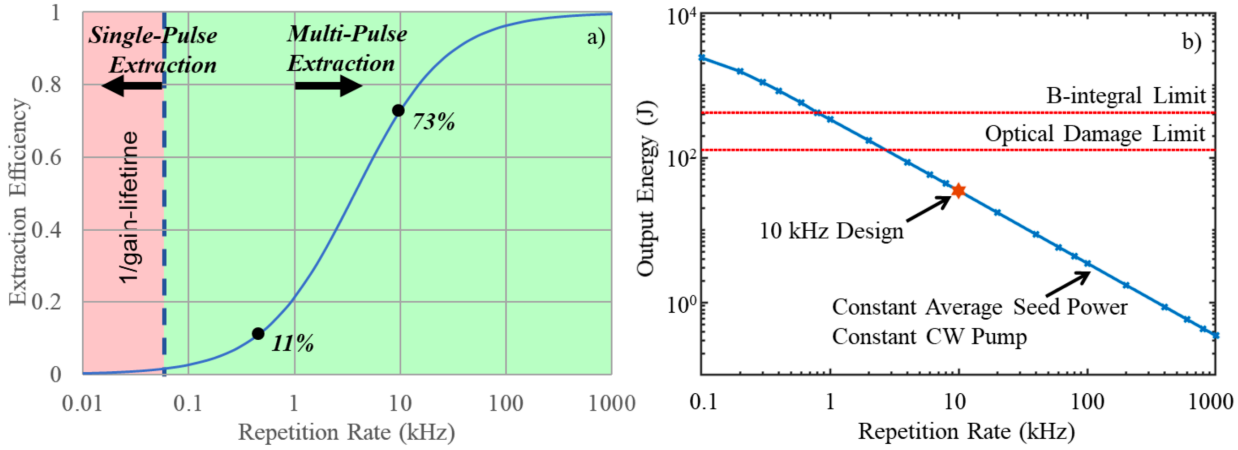

Figure 1.2: Left: Plot showing the extraction efficiency gains when switching to multi-pulse extraction, especially at the high repetition rates needed for EUV lithography in high volume manufacturing settings. Right: Plot showing the tradeoff between output energy per repetition and the repetition rate. [11]

the ratio of 13.5 nm +/- 1% light output on a half-sphere backwards to the laser over the input laser energy.

ASML, the only company manufacturing high volume manufacturing (HVM) compatible EUV machines, currently uses a CO2 laser in its source to drive the LPP process. This decision was a culmination of extensive debate in the 2000s and early 2010s, with many papers published showing evidence for and against CO2 lasers and shorter-wavelength solid-state lasers. [9-11] Eventually, the CO2 laser won out because of its technological availability at high frequencies and laser power, both necessary for EUV lithography to be economically viable. Currently, the CO2 laser is driven at a laser intensity of ~10^9 W/cm^2 and a repetition rate of 50,000 Hz, totaling a laser power of up to 40 kW. [12] With the range of technological improvements ASML has implemented in its machines over the years, such as dual pulse irradiation, advanced target formation, and the master oscillator power amplifier, its latest EUV scanners boast a conversion efficiency of up to 6%. [12]

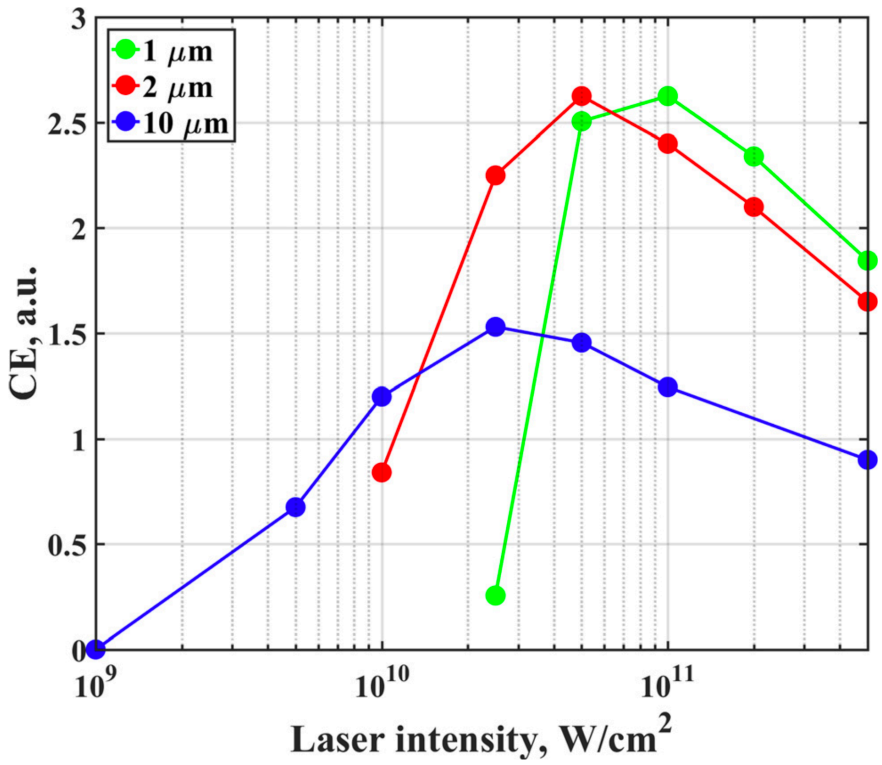

Figure 1.3: Plot showing the relationship between conversion efficiency, laser intensity, and laser wavelength for a single pulse irradiation scheme. In the shift to shorter wavelength, solid-state lasers, a higher laser intensity is required to achieve the maximum conversion efficiency capable. [21]

In recent years, there has been increased attention in solid-state lasers as an alternative to the existing CO2 laser system. [13] The switch to solid-state lasers promises a smaller physical footprint, improved wall plug power efficiency, better pulse shaping capabilities, and more efficient energy deposition into the plasma. The argument for a switch to solid-state has been further bolstered by the introduction of two new laser systems, the Big Aperture Thulium Tm:YLF-based 2-micron wavelength laser and the SHARC Nd:glass 1-micron wavelength laser. [14] These lasers, which utilize continuous pumping and multi-pulse extraction to circumvent the thermal issues relating to high power operation, are designed to operate at the repetition rates and powers needed for HVM EUV scanners. While still in the early design stage, the former is

estimated to provide 1 J doses at 100 kHz repetitions, while also showing minimal pulse distortion and good pulse-to-pulse stability. [15]

One challenge with moving to 1-or-2 micron wavelength laser systems is the difference in their resulting plasma compared to that of the 10 micron CO2 laser. Most evidently, a switch over to shorter wavelength lasers changes the parameter space needed for ideal 13.5 nm light creation, requiring higher intensities of about 1.4e11 W/cm^2 — nearly two orders of magnitude greater than what is required with CO_2 systems. [13] The wavelength dependence on peak laser intensity can be seen in Figure 1.3. Additionally, while a shorter wavelength laser tends to be more easily absorbed into the plasma by virtue of its higher critical density, the resulting plasma is denser, making the self-absorption of 13.5 nm light a more significant issue. [16] This effect, known as opacity, broadens the resulting spectra and limits the maximum attainable conversion efficiency. [17] As a result, even varying the laser parameters across a wide range of laser pulse durations, droplet sizes, and laser intensities, a peak conversion efficiency of only 3.2% was achieved in the most comprehensive optimization work done to date — a far cry from the 6% achieved by ASML's dual pulse system. [13]

The research-to-date into solid-state laser systems only underscores the importance of continued research and breakthroughs to surpass the existing CO2 systems. However, such research is often costly, inaccessible, and slow. As such, computer simulations that model the expansion and the spectral production of the plasma can be helpful to estimate the effect of parameter changes before committing to experiments or hardware changes. A wide range of software packages have been used in the literature to this effect. The HEIGHTS integrated software package, used by researchers at the Center for Materials Under Extreme Environment at

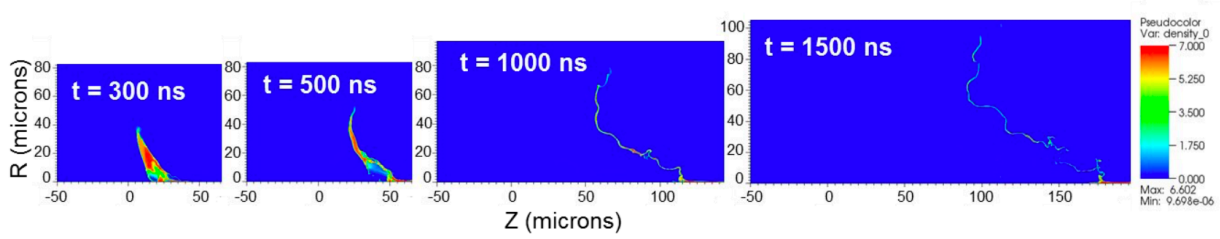

Figure 1.4: Simulated time evolution of a low-intensity prepulse-irradiated tin droplet. [22]

Purdue University, has been used to study the effects of, among other things, pulse duration, laser wavelength, plasma spatial profile, and prepulse wavelength on EUV output. [18-21] HYDRA, a 3D radiation-hydrodynamics code base developed at Lawrence Livermore National Laboratories, has been used alongside an ALE-AMR code to model the prepulse and main pulse interactions with a tin target. [22] The combination of RALEF2D and THERMOS has been used to optimize the CE of an Nd:YAG-prepulse-CO2-main-pulse system. [23] FLASH code, the simulation code base used in this paper, has been used in tin LPP simulations prior to this paper, albeit with just planar tin targets and a limited parameter space. [24] As such, the combination of FLASH and SPECT3D, while not new in plasma physics simulation, has not been used together in modeling a solid-state laser, tin droplet target EUV source.

As useful as simulations have been in the past, a common through line across the literature is the imperfect replication of experimental spectra, attributed in a landmark paper from 2019 to the imperfect modeling of multiply-excited states in rudimentary atomic models. [25] However, detailed spectra modeling of the kind used in Reference 25 is computational expensive and requires access to proprietary atomic modeling packages. To complicate things further, the dual pulse irradiation scheme, which involves a lower energy prepulse to decrease the density of the plasma followed by a main pulse that produces the bulk of the 13.5 nm light, and which is

now an industry standard method for improving the conversion efficiency and reducing the tin debris produced, is difficult to model accurately because of its large temporal (fractions of a nanosecond to microseconds) and spatial (10s of nanometers to 100s of microns) ranges. [22]

In short, there is a need for an accessible yet accurate method for simulating the plasma expansion and EUV output of laser-produced tin plasma.

1.2 Thesis Outline

The research presented in this thesis involves simulations of the expansion and resulting EUV output of a laser produced tin plasma. In this study, we benchmarked FLASH and SPECT3D, two tools with minimal use so far for modeling EUV lithography, against results from Reference 13, a comprehensive 1 micron optimization study from 2019. After finding good matching of spectra between simulation and experiment, we introduced 4 novel pulse shapes to the EUV literature — step down, step up, Gaussian ramp, and mini-prepulse — and tested their conversion efficiencies against existing pulse shapes.

The first chapter introduces the reader to the state of play of lasers in EUV sources; recent arguments for and against the shift towards solid state lasers; and simulations in EUV lithography. The second chapter details the two simulation tools used — FLASH and SPECT3D — used in this work. The third chapter includes a straightforward comparison between the simulated results and the results from an experimental study; modifications to improve the spectral profile matching between simulation and experiment; and explanations to any remaining differences between the simulated and experimental spectra. The fourth chapter compares the effect of temporal pulse shaping on conversion efficiency using both commonly used profiles

and novel profiles. The fifth and final chapter concludes the thesis with a summary of the work and recommendations for future work in EUV simulations.

Chapter 2. FLASH and SPECT3D as Simulation Tools

2.1 Introduction

As processing speeds have gotten faster year-on-year, a wide range of plasma simulation tools have sprung up over the last two decades. Now, researchers in plasma physics have a dazzling array of tools to choose from. In this study, we chose FLASH and SPECT3D, the former an open-source codebase and the latter a commercially available piece of software, to simulate the expansion of tin plasma upon irradiation by a 1 micron laser and its resulting light output. Internally, FLASH and SPECT3D were natural picks for the simulation tools because they were already used in our lab for other purposes. Additionally, unlike many of the other tools in the literature, FLASH and SPECT3D are not restricted by geographical region, institutional access, or connections to a National Laboratory. As such, these tools are some of the most easily accessible tools to study EUV lithography — perfect for new researchers into the field.

2.2 FLASH Code

FLASH code, developed by the FLASH Center for Computational Sciences at the University of Chicago, as a modular, parallel, multiphysics code framework for simulating plasma physics and astrophysics flows. [26, 27] Using three-temperature (3T) radiation-hydrodynamic equations, multigroup diffusion (MGD) radiation transfer, tabulated equation of

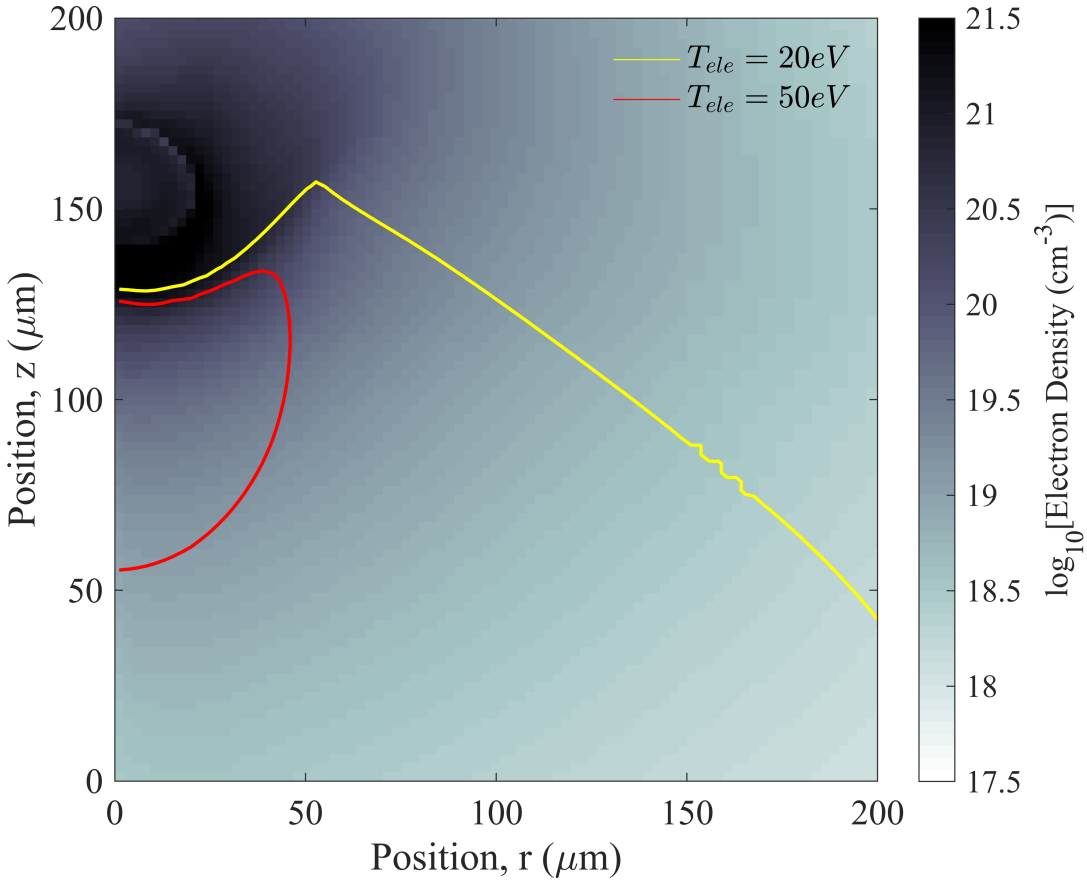

Figure 2.1: Electron density distribution plot from a FLASH "plt_cnt" output file at the 10 ns time step. The parameters used for this simulation are similar to those used in later sections, with a laser intensity of 1.4×10^{11} W/cm^2, total pulse duration of 15 ns, and laser spot size of 96 μm. Two temperature contours — 20 eV and 50 eV — are overlaid on the plot to indicate the region bounded by the ideal plasma temperature to produce 13.5 nm light.

state (EOS), tabulated opacity, and electron thermal conduction, LaserSlab, an application within the FLASH computing package, allows for laser-driven high energy density physics (HEDP) experiments in which one-or-more high-powered laser irradiates a chosen target.

In the laser driven plasma process used in EUV lithography, inverse bremsstrahlung — the transfer of photon energy into via electron-ion collisions when a photon-absorbed electron encounters an ion — is the primary method by which laser energy is deposited into the tin target and plasma. In LaserSlab, inverse bremsstrahlung is modeled by separating the full laser beam

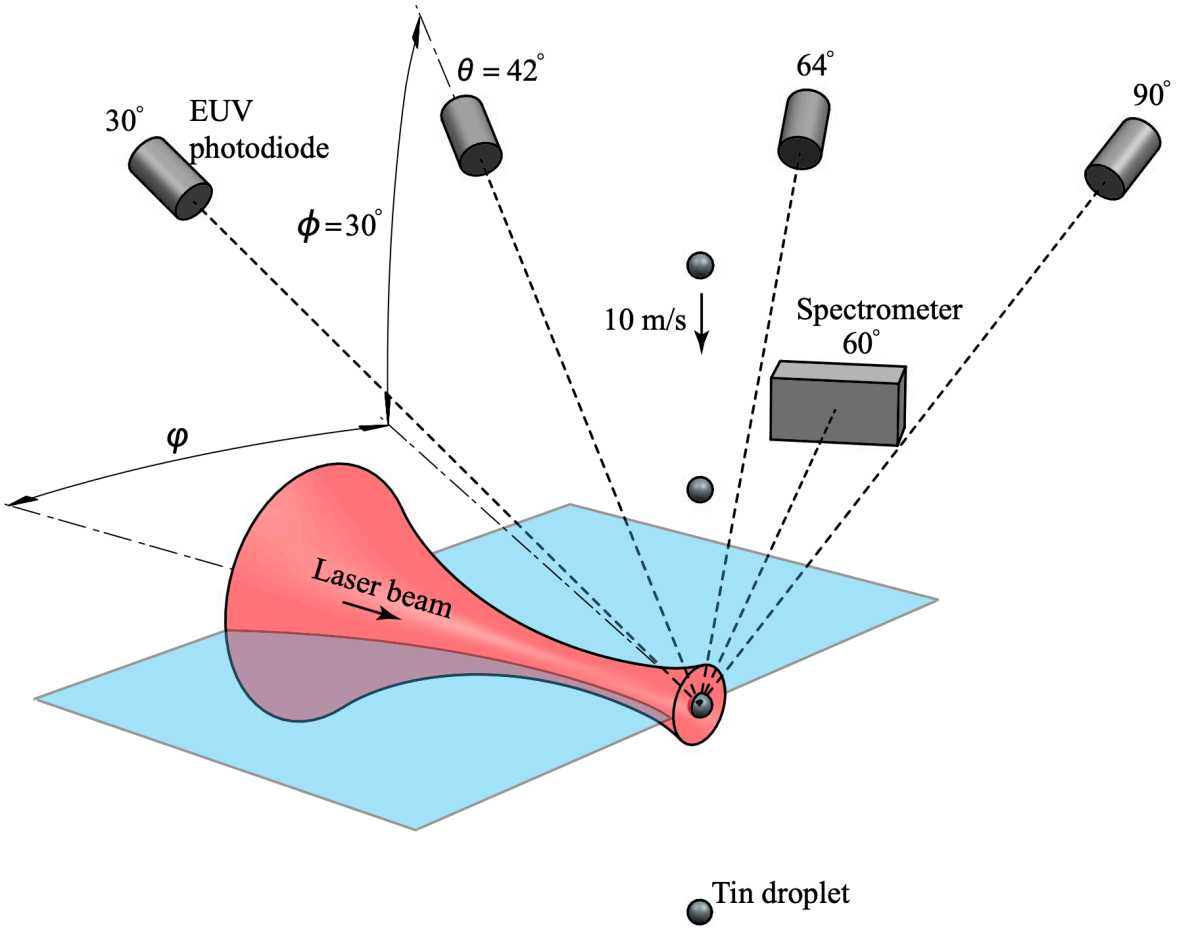

Figure 2.2: Experimental setup from the benchmarked study showing the array of photodiodes at different angles and the spectrometer at 60 degrees from the plane of the laser. As in the experiment, only the 30 degree photodiode and the spectrometer were simulated to calculate the conversion efficiency and resolve the spectral output respectively. [13]

into individual rays and interpolating the energy deposition at each time step. Then, using inverse Bremsstrahlung approximation equations and 3T equations, the laser energy transferred to electrons and ions in the plasma respectively are calculated. Further detail into the specific equations and calculations in LaserSlab are described in Reference 28.

Because the opacity and EOS tables for tin and hydrogen gas were not included in a stock installation of FLASH, we used PROPACEOS to generate them. The files generated by PROPACEOS were first converted to the IONMIX4 file format for use with FLASH. With the

tables, along with the laser parameters, target parameters, chamber parameters, mesh sizes, and boundary size, a ".par" setup file was created. The experimental parameters used were based on those used in Reference 13. While many of the laser parameters were changed throughout the experiments, the following parameters were kept constant throughout: 1.06 micron laser wavelength, 46 micron tin droplet diameter, and 2D cylindrical coordinates.

A simulation in FLASH produces two output files at defined time steps, the "plt_cnt" file and the "chk" files. The former includes just the basic information about the simulation time step such as densities, temperatures, and laser energy deposition; the latter includes all the information collected by FLASH at that time step such that the simulation can be restarted with just that file. A sample output at the 10 ns time step using parameters similar to that used in later sections is displayed in Figure 2.1.

2.3 SPECT3D

To produce the spectral profile from FLASH, we used SPECT3D [29], a multidimensional spectral analysis software, to process the output files from FLASH into spectral data. SPECT3D calculates the emission, absorption, and ionization properties of the plasma, which are then converted into spectral fluxes by virtual detectors. The process of importing the FLASH output into SPECT3D involved selecting the "chk" files and specifying the chamber material fraction, target material fraction, temperature variable, density variable, and the atomic materials involved.

A number of changes were made to the default options on SPECT3D to obtain an accurate spectra. Firstly, the atomic model used throughout the SPECT3D runs was the preconfigured "Emission Visible/UV/EUV Spectroscopy", which provided the best results for

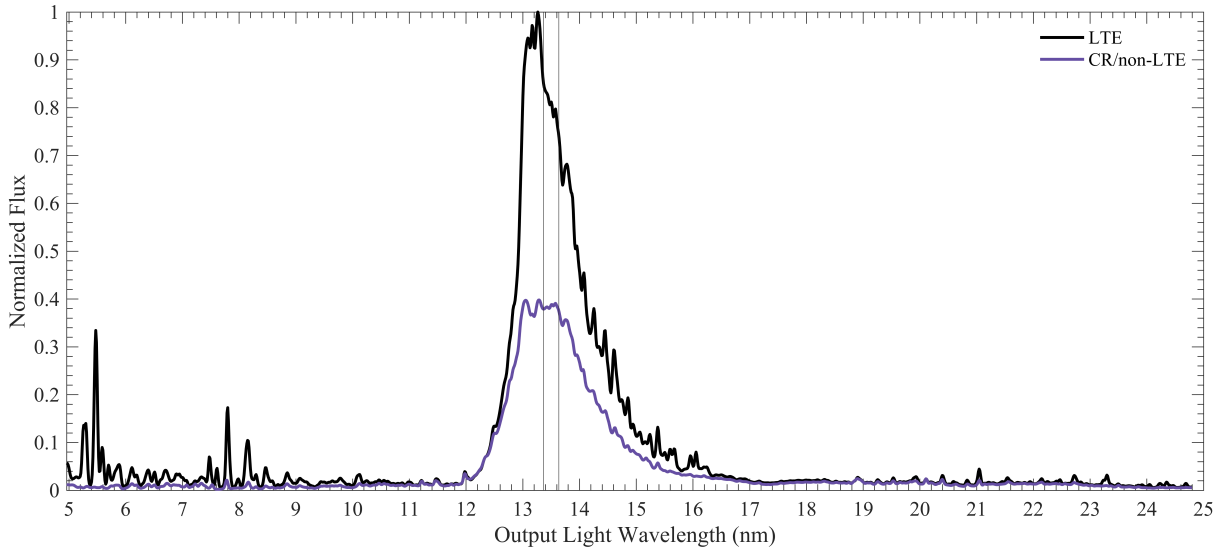

Figure 2.3: Comparison of the flux outputs with LTE and CR (non-LTE) models at the 10 ns time step. The two vertical bands represent the bounds of the "in-band" radiation — light within the 2% bandwidth around 13.5 nm.

the range of spectra relevant in this study. Similar to the experimental setup (reproduced in Figure 3.2) used in the paper mentioned, in SPECT3D, the obtained spectrum was recorded by placing a virtual detector at 60 degrees from the axis of the incoming laser and the conversion efficiency was calculated using the spectrum obtained by a virtual detector at 30 degrees azimuthally and polarly from the axis of the incoming laser. [13] This ability in SPECT3D to place virtual detectors in 3D space according to the experimental setup, allows for an apples-to-apples comparison of the output spectra that is new to the literature.

Before we processed all the FLASH output files, we first processed a 1.4×10^{11} W/cm^2 laser intensity run in SPECT3D at the 10 ns time step as described in Section 2.2 using both the default Local Thermodynamic Equilibrium (LTE) and the Collisional-Radiative (CR) kinetic models to verify the validity of the LTE approximation. We found that the CR model, which forgoes the more simple Boltzmann-and-Saha-equation-based LTE in favor of multi-level atomic rate equations, produced a spectral profile that is markedly different from that using the LTE

model. As evident in Figure 3.3, the CR model resulted in a shorter and slightly left-shifted peak. If the LTE approximation were valid, the CR model would result in a spectrum that looked similar to the LTE model. As such, with the shorter-wavelength, single pulse, 10^{10} — 10^{11} W/cm^2 intensity laser produced tin plasma simulations carried out in this study, the LTE approximation is invalid, and all simulations henceforth use the CR model.

We made a few assumptions in the following calculations to simplify the simulation process. Firstly, the tin droplet target was assumed to be stationary, instead of moving out of a droplet generator. We believe this assumption to be valid as the time scales involved in the single pulse experiments are small. Secondly, the background gas density of the hydrogen-filled chamber was assumed to be 1×10^{-5} g/cm^3 — the lowest required for simulation stability. In a comparison with lower chamber pressures, this density was found not to affect the laser, plasma expansion or the resulting spectra.

Chapter 3. Benchmarking FLASH and SPECT3D Against Published Experimental Results

3.1 Introduction

Simulations have been used widely in the literature to study the effects of laser parameter and target parameter changes to the EUV output of the plasma. However, much of the research published in EUV simulations involved tools other than those used in this study, many of which are restricted or proprietary to institutions or national laboratories. Additionally, benchmarking of the software packages used is often incomplete, involving just the matching of conversion efficiency trends, in some cases even excluding a benchmark completely. While FLASH and SPECT3D have been used for simulating EUV sources prior to this study, use of the combination has been limited in both input and output. [24] With respect to the former, the single study involving FLASH and SPECT3D only used a slab target and a CO2 laser; with respect to the latter, neither a benchmarking process for accuracy verification nor an analysis of the spectral output were undertaken.

In this chapter, we compared FLASH and SPECT3D to an existing set of 1 micron laser, droplet target results by studying the similarities and differences between their output spectra, output energies and conversion efficiencies. [13] As in Section III-A of Reference 13, we kept

constant a laser wavelength of 1.06 micron, a total pulse duration of 15 ns, a laser spot diameter of 96 μm, and tin droplet diameter of 46 μm, while varying the laser intensities in 5 steps between 0.1×10^{11} W/cm^2 and 2.7×10^{11} W/cm^2. The spectral profile was obtained with a virtual detector at 60 degrees from the plane of the laser, while the output energy, and, thus, conversion efficiency, was obtained with a virtual detector at 30 degrees from the plane of the laser.

3.2 Benchmark Results

To benchmark the performance of FLASH and SPECT3D, we take the novel approach of comparing the simulated spectra with that from a set of experimental data. As seen in Figure 3.1, the simulation results' peaks mirrored the experimental results' peaks in important ways. Most significantly, with the higher laser intensities, both plots showed peaks at-or-around the 13.5 nm wavelength, indicating that SPECT3D was able to model the tin plasma spectra with a good baseline level of accuracy. Furthermore, the simulation peaks shifted leftward into the 13.5 nm bandwidth as laser intensity increased from 0.1×10^{11} W/cm^2 to 0.6×10^{11} W/cm^2, mirroring the trend in the experimental peaks. Lastly, as laser intensity was increased, the simulated peaks narrowed, matching what was observed experimentally.

However, the simulated peaks also differed from the experimental peaks in significant ways. Most obviously, the simulated peaks did not reside at the same positions as the experimental peaks. In the experimental results, the three highest intensity plots all peaked within the 13.5 nm bandwidth, with the peaks narrowing as laser intensity increased. On the other hand, in the simulated results, the four lowest intensities peaked to the left of the experimental results, with the 0.3, 0.6, and 1.4×10^{11} W/cm^2 plots peaking even to the left of the 13.5 nm bandwidth. Even more strangely, the highest intensity plot, 2.7×10^{11} W/cm^2, shifted

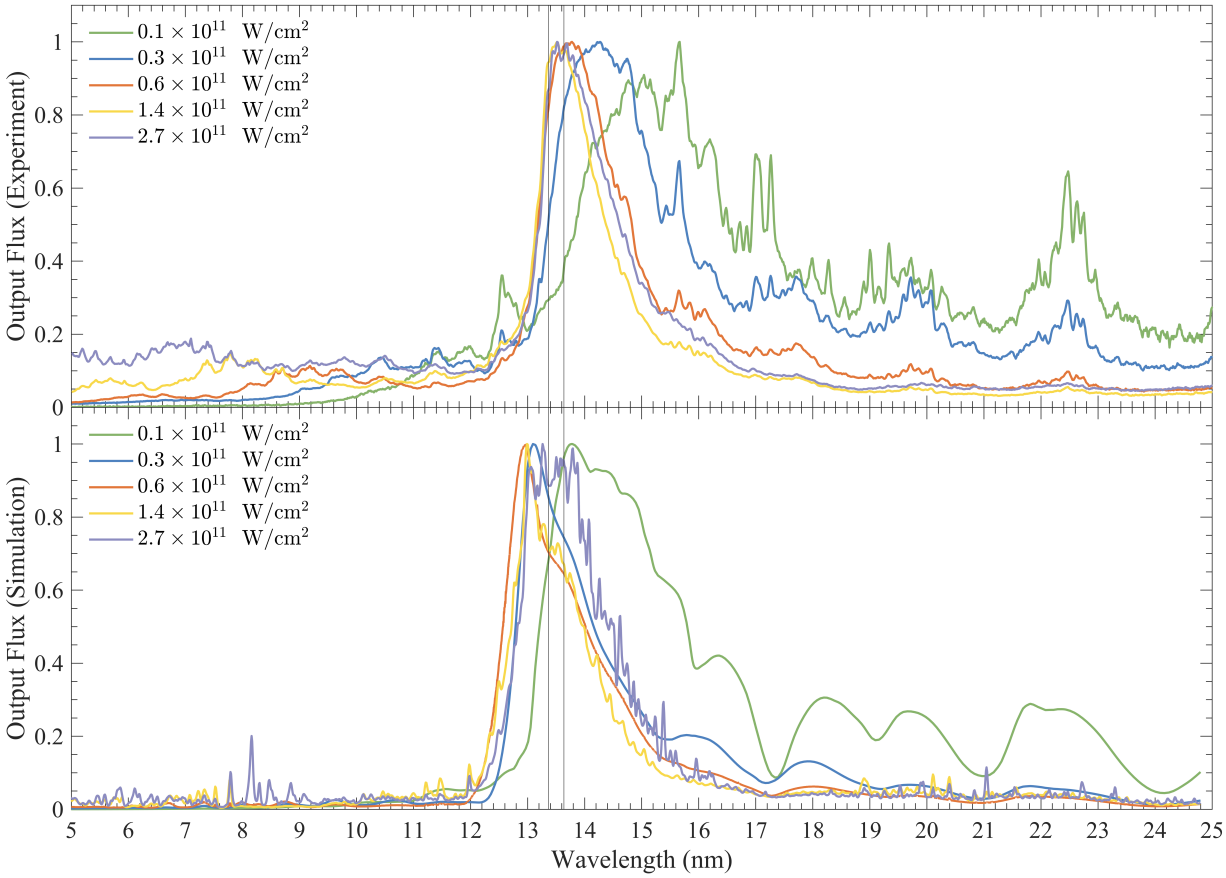

Figure 3.1: Top: experimentally obtained output spectra for a 1.06 micron laser with a 15 ns pulse duration, 96-μm diameter laser, 46 μm diameter droplet at 5 different laser intensities. Bottom: Output spectra obtained by simulation with FLASH and SPECT3D at the same parameters as the experimental data. The two vertical lines represent the bounds of the 2% bandwidth around 13.5 nm, the "in-band" region.

back to the right and was centered within the 13.5 nm bandwidth. This "V-shape" trend, observed experimentally in other studies [30] albeit to a lesser degree, was not observed in the study benchmarked. Last but not least, the simulated curves had a narrower bandwidth across all intensities measured compared to the experimental curves.

While the spectral peak is the most important feature to get right for conversion efficiency calculation purposes, the non-peak, out-of-band regions are also worth analyzing. Staying on Figure 3.1, we see that the simulation captured the lower (4+, 5+, 6+) ionic level

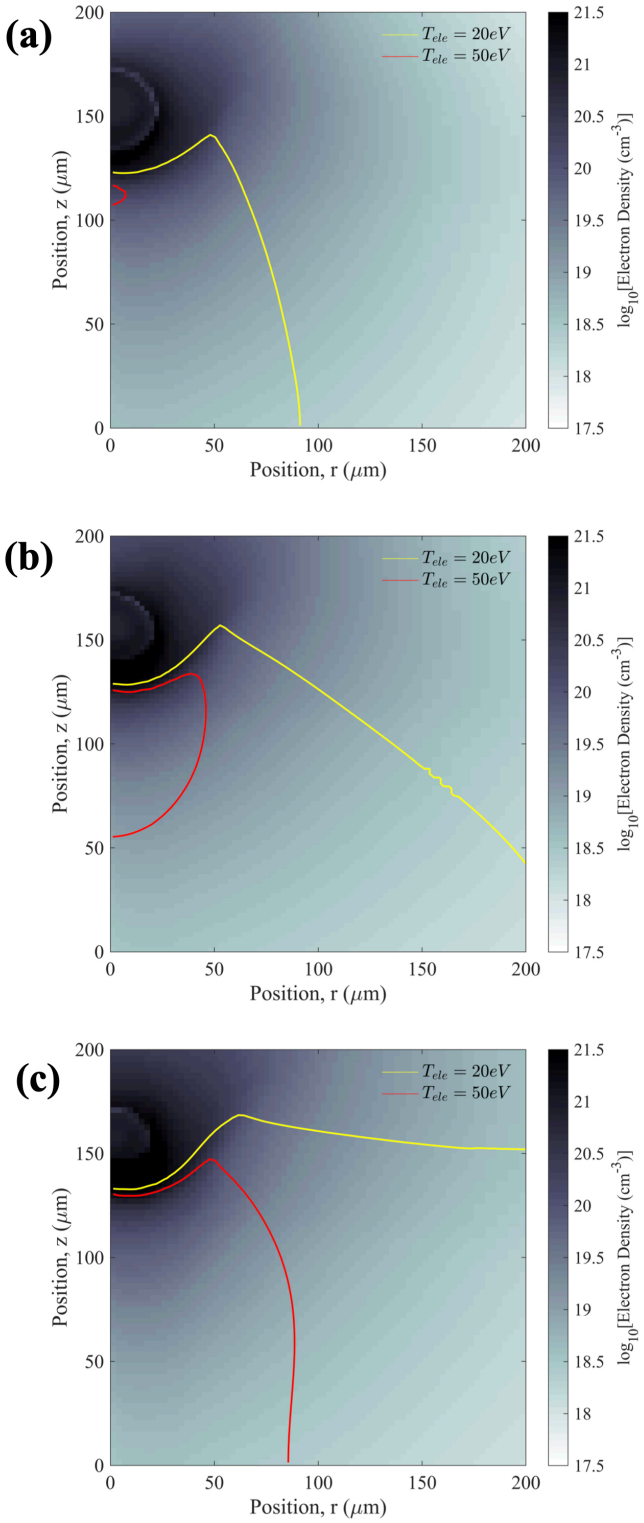

Figure 3.2: Spatial distribution of electron density at three different laser intensities: (a) 0.6×10^{11} W/cm^2, (b) 1.4×10^{11} W/cm^2, and (c) 2.7×10^{11} W/cm^2. The purple and blue contour lines represent the temperature contours at 20 eV and 50 eV respectively, indicating the bounded region of high EUV-emitting plasma.

features and higher (13+, 14+, 15+) ionic level features well, as seen in the super-15 nm features of the 0.1×10^{11} W/cm^2 plot and in the sub-10 nm features of the 2.7×10^{11} W/cm^2 plot respectively. In both the sub-10 nm and super-15 nm cases, the peaks appeared at similar wavelengths, indicating that SPECT3D was able to image the full range of ionic levels well. However, the simulated out-of-band features occupied a smaller relative proportion of the overall spectra than the experimental spectra. This result, along with the left-shifted peaks described in the previous paragraph, indicates that the simulation behaved as if the laser intensity was higher than it actually is — a higher "effective laser intensity".

Now digging into the spatial distribution of plasma density and temperature in Figure 3.2(a)-(c), we observed that the size of ideal EUV-producing plasma — plasma with a temperature between 30 eV and 70 eV and an ion density between 10^{17} and 10^{18} cm^{-3} [8] — increased with increasing laser intensity. This is seen in the plots as the overlap between the density and temperature contours increased going from 0.6×10^{11} W/cm^2 to 2.7×10^{11} W/cm^2. In fact, output in-band energy increased exponentially with increasing input laser intensity within the range measured, showing a straight line trend in the logarithmically-scaled normalized output in-band energy vs input laser intensity plot seen in Figure 3.3.

Conversion efficiency, the primary performance metric used for EUV production, is another aspect of the simulated results that compares and contrasts with the experimental results in an interesting way. In the simulations carried out, the conversion efficiency was calculated using the following equation:

$$CE = \frac{\int_0^{\tau_L} \phi_{13.5\ nm}(t)dt \times \pi r^2}{I_L \tau A_L} \qquad (1)$$

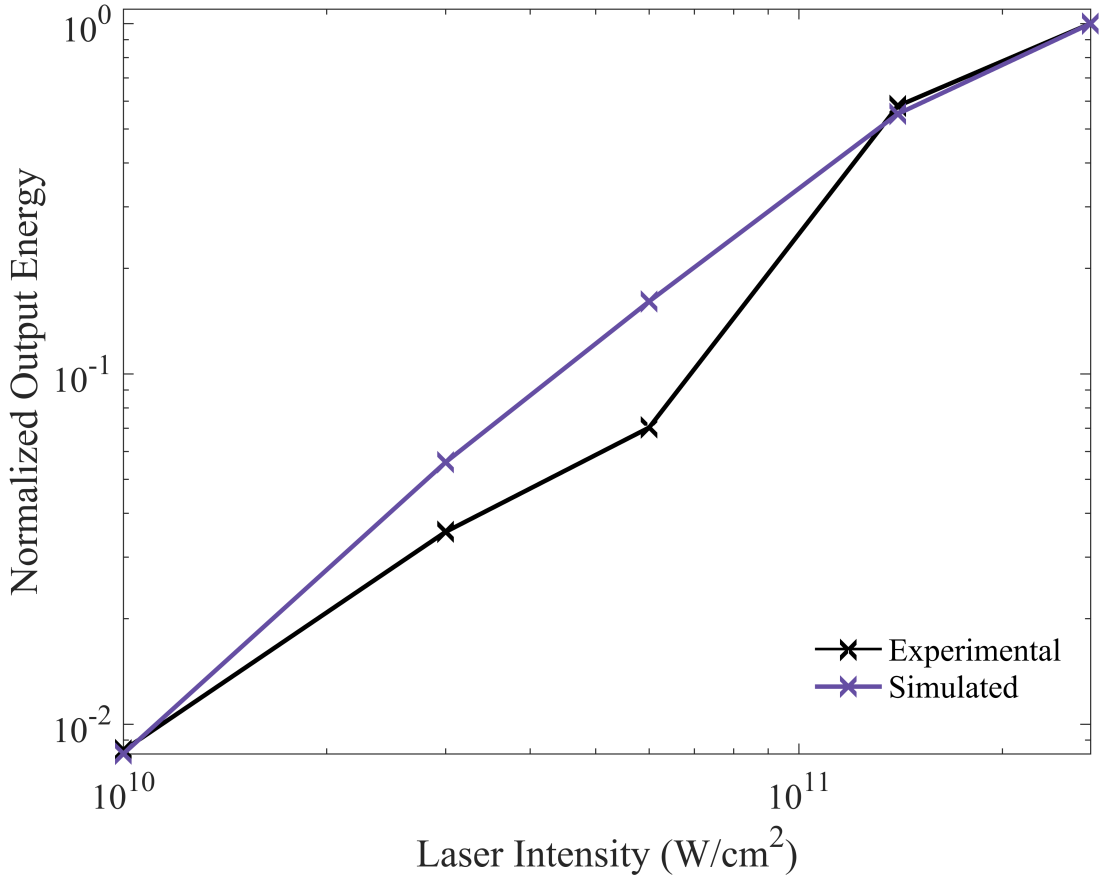

Figure 3.3: Dependence of laser intensity on the output energy for a 1 micron laser-irradiated tin droplet, both by simulation and by experiment.

for time-integrated in-band flux density at detector, $\phi_{13.5\ nm}$, pulse duration, τ_L, distance from detector to target, r, laser intensity, I_L, and laser spot area, A_L. Similar to the simulated normalized energy profile, the simulated normalized conversion efficiency profile followed the trend of its experimental counterpart, as seen in Figure 3.4. However, sans normalization, the spectra tell a different story: the conversion efficiency obtained by simulation was higher than that by experiment at each intensity level. In the optimal case — a laser intensity of 1.4×10^{11} W/cm^2 — the simulated CE was 2.6% while the experimental CE was 1.8%. At other laser intensities, the simulated CEs saw commensurate improvements over the experimental CEs as

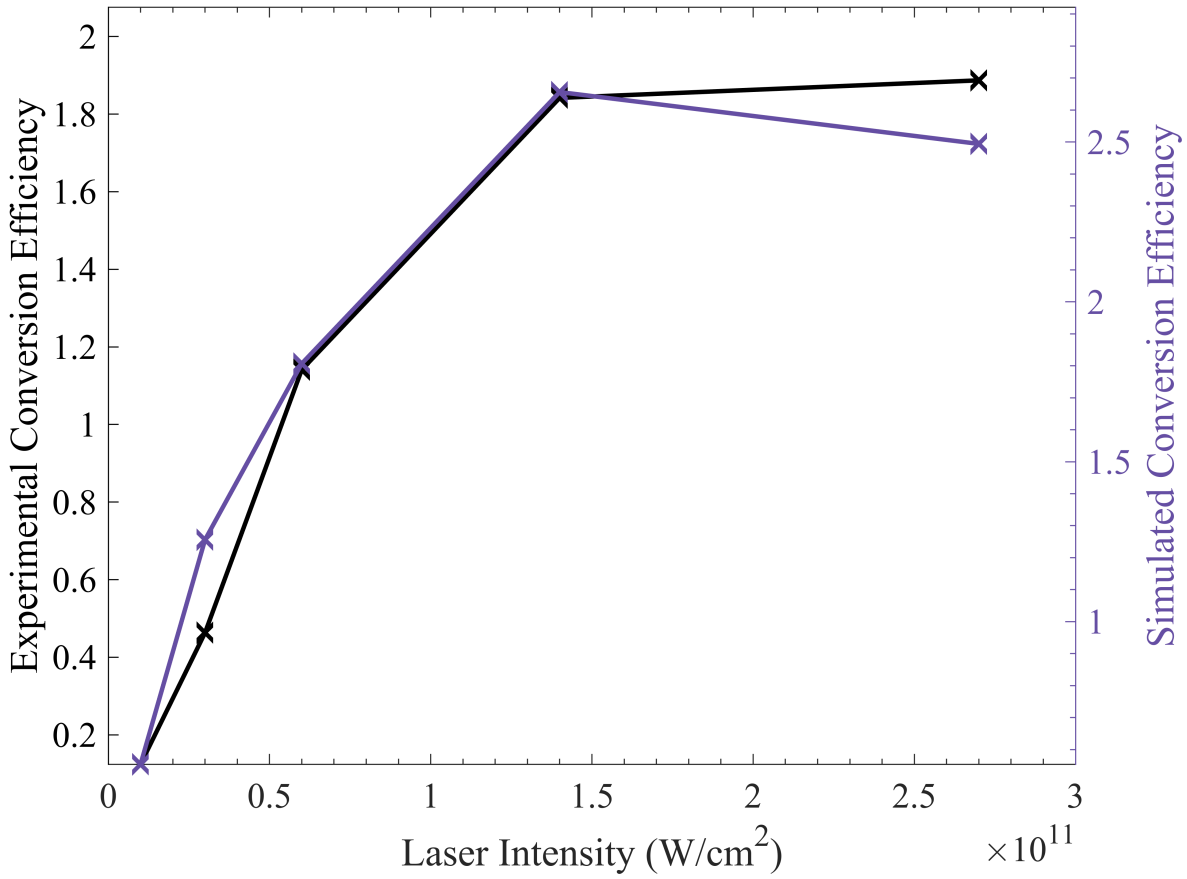

Figure 3.4: Plot of experimental and simulated conversion efficiency against laser intensity.

well. This, in combination with the fact that the simulated CE peaked at 1.4×10^{11} W/cm^2 while the experimental CE peaked at 2.7×10^{11} W/cm^2, further bolsters the idea that the simulation results displayed a higher "effective intensity" than the experimental results.

3.3 Modifications to Improve Spectra Matching

In the previous section, owing to the left-shifted peaks, higher conversion efficiency, and higher "effective laser intensity", we found that the combination of FLASH and SPECT3D was in its stock configuration was not able to perfectly replicate the experimental spectra. In the interest of correcting for those differences, we reduced the simulated laser intensity down by approximately a factor of two and artificially shifted the curve rightwards by 0.55 nm, resulting

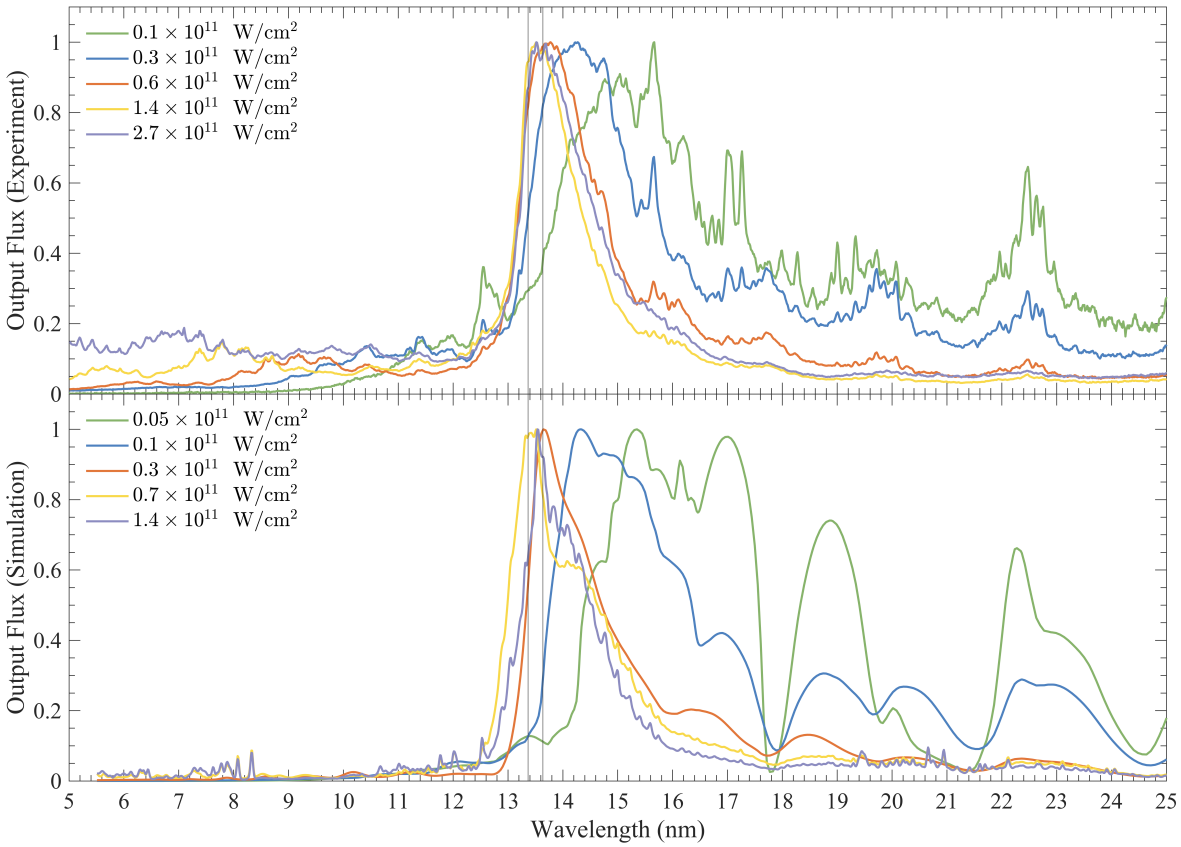

Figure 3.5: Top: experimentally obtained output spectra for a 1.06 micron laser with a 15 ns pulse duration, 96-μm diameter laser, 46 μm diameter droplet at 5 different laser intensities. Bottom: Output spectra obtained by simulation with FLASH and SPECT3D after adjusting for laser intensity and applying an artificial right-shift of +0.55 nm. The top vertical lines represent the bounds of the 2% bandwidth around 13.5 nm.

in a normalized spectral profile that more closely matched the experimental one as seen in Figure 3.5.

With the changes described, spectra matching between the simulation and the experiment improved in the peaks — the part of the spectra most relevant to in-band EUV production and conversion efficiency. Most noticeably, the peak wavelengths were better matched, with the three highest intensity plots calling squarely in the in-band 13.5nm region and the two lower intensities falling just to the right of that region. The trends of bandwidth narrowing and "V-shape" peak wavelength with increasing intensity were also maintained from the initial

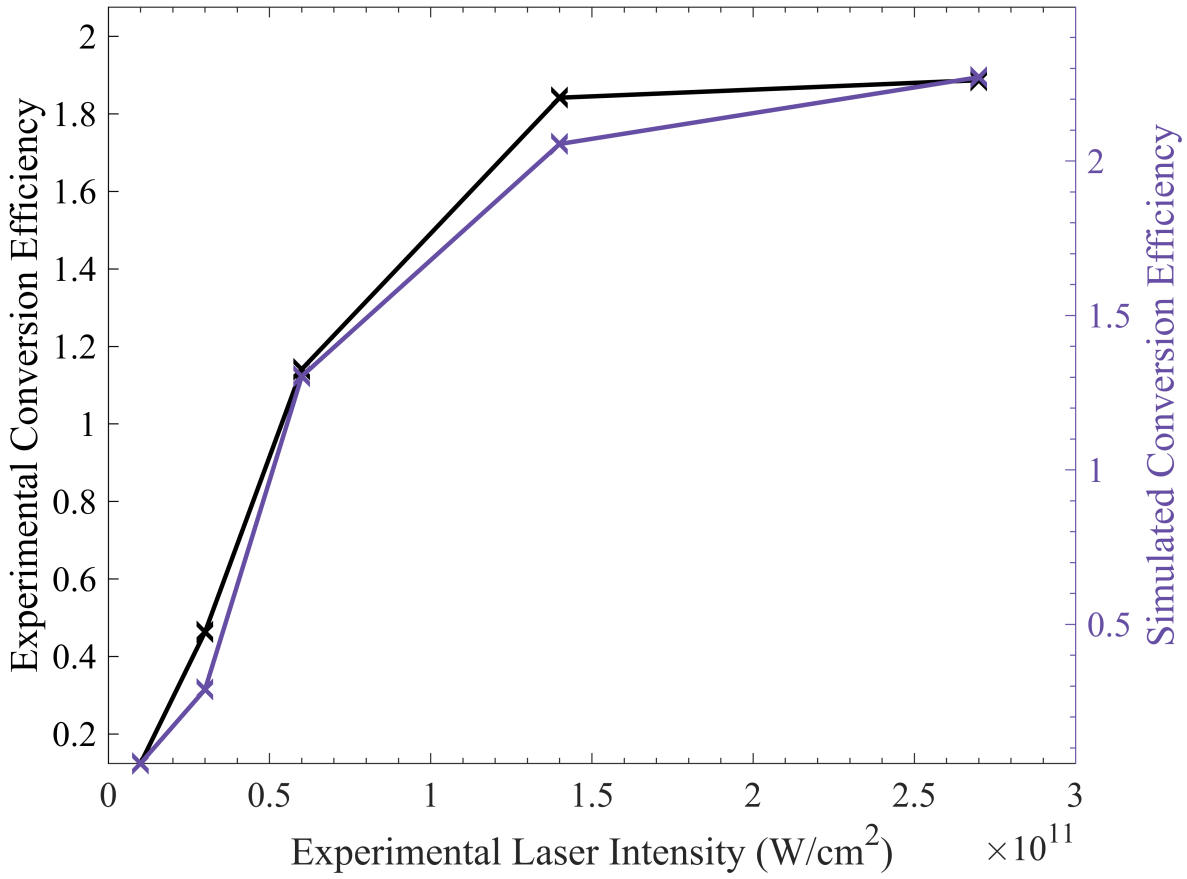

Figure 3.6: Plot of the experimental and the spectra-matched, simulated conversion efficiency against experimental laser intensity.

benchmarking plot, lending confidence to the validity of the changes made. The conversion efficiency of the matched spectra, plotted in Figure 3.6, also showed improvements in accuracy, maintaining some of the profile accuracy while skewing closer on an absolute scale, too.

However, there remain some significant, unresolved differences between the experimental and simulated plots. Similar to the initial benchmarking plot in Section 3.2, the bandwidth of the simulated peaks were narrower than that of the experimental peaks. The modeling of the out-of-band regions also remain inaccurate, showing much less detail at the lower ionization levels of tin and proportionally much less spectral intensity at the higher

ionization levels. Potential explanations for these differences are detailed in the discussion in Section 3.4.

3.4 Discussion

One consistent difference between the simulated and experimental plots was the difference in peak bandwidth, in which the simulated bands were consistently narrower than the experimental bands. This could be attributed to an under-modeling of opacity — the transmissibility (or lack thereof) of desired light through the plasma — in SPECT3D. Experimentally, the primary effects of opacity on the in-band 13.5 nm output light was the flattening and broadening of the peaks, as found experimentally by varying the thickness of tin. [17] If this theory were to hold, it would explain the higher conversion efficiency obtained by simulation because less of the desired light is reabsorbed by the plasma.

One explanation for the persistent undermodeling of opacity in SPECT3D is the same ill that plagues other spectral simulation tools: the failure to fully take into account multiply excited states. [25] In a recent study of opacity in simulations, transitions between states were found to dominate the opacity of the plasma, a radically different conclusion from the consensus view that opacity comes primarily from one-electron-excited states. Currently, access to ATOMIC, the atomic level calculator used in Reference 25, is restricted, making it difficult to incorporate the multiply excited states modifications made into this study.

In addition to the reduction in intensity and artificial right shift used in the previous section, we tinkered with the various spectrum-affecting options in SPECT3D such as turning on multiply excited states, altering rate coefficients for certain transitions, changing the rate modifiers, using different atomic models, among others. Unfortunately, we found that all of the

options tested resulted in either little or no change in the resulting spectra, in some cases even resulting in a less accurate spectra. Included in the Prism software package is the ability to reconstruct an alternate atomic model through its AtomicModelBuilder application, however such work requires detailed knowledge of the specific transitions of tin and thus is outside the scope of this study.

Despite the marked improvement in spectra matching with the above interventions, we advise that the methods employed here be used with precaution. The spectra matching carried out in this study only involved a small subset of the larger study in Reference 13, and as such is not representative of the entire 1-micron laser-produced tin plasma parameter space. Furthermore, because experimental laser intensities and spectrometer calibration can vary slightly from experiment to experiment, the data borrowed from Reference 13 may be subject to inconsistencies as well. As such, further, repeated benchmarking is needed across the parameter space to improve the robustness of and confidence in FLASH and SPECT3D for absolute EUV simulation purposes.

Chapter 3, in part, is currently being prepared for submission for publication of the material. Lee, Brian; Matsuo, Kazuki; Bailly-Grandvaux, Mathieu; Beg, Farhat. The thesis author was the primary investigator and author of this material.

Chapter 4. Effects of Pulse Shaping on Conversion Efficiency

4.1 Introduction

A move from CO2 lasers to shorter-wavelength solid state lasers has the potential to bring with it improved temporal pulse shaping capabilities. [15] Pulse shaping — the precise control of laser power over the duration of the pulse through a pulse synthesizer — is essential to optimal laser-driven inertial confinement fusion, but has not been given much attention in EUV lithography. In a recent paper testing 6 different pulse shapes — square, Gaussian, triple Gaussian, quintuple Gaussian, up-ramp, and down-ramp — the square pulse resulted in the highest CE. [26] However, the mere six different pulse shapes studied do not fully encompass the radically expanded parameter space afforded by improved pulse shaping capabilities. As such, there is a need for novel pulse shaping methods and further optimization work to fully take advantage of the new laser systems.

In preparation for a move towards solid state lasers, and with the confidence in benchmarking from Section 3, we tested the following pulse shape profiles: square, fixed duration Gaussian, fixed peak-intensity Gaussian, step down, step up, Gaussian ramp up, and mini-prepulse. In the interest of distinguishing between the performance of well-established laser

profiles and the performance of the novel pulse shapes introduced here, we separate analysis of the first three pulses from rest in Section 4.2. We then follow the first three pulses up with novel pulse shapes, described in Section 4.3, based on the learnings from the basic pulses. We conclude the chapter with caveats and future work recommendations in temporal pulse shaping.

4.2 Common Pulse Shapes at Constant Energy

In the first group of pulses — square, fixed peak intensity Gaussian, and fixed duration-Gaussian — we controlled for a laser energy of 0.152 J and based the other parameters off the peak CE case in Section 3.3. The square pulse was identical to the 1.4×10^{11} W/cm^2 intensity, pulse used in Section 3.3; the Gaussian pulse used the same peak intensity as the square pulse with a FWHM duration of 16.66 ns; the high-peak Gaussian pulse used a higher laser intensity of 3.3×10^{11} W/cm^2 with the same total pulse duration as the square pulse. The pulse profiles for all three is displayed in Figure 4.1. After processing the FLASH outputs in SPECT3D, the resulting spectra were shifted in wavelength by +0.55 nm as done in Section 3.3.

Curiously, as seen in Figure 4.2, the in-band EUV output profile followed the pulse shape closely. In the two Gaussian profiles in particular, in-band output power production very closely traced the input power, showing, at least for the peak conversion efficiency energy case used in this section, that input power is correlated to output power. Of the three plots, the fixed duration Gaussian profile achieved the greatest peak output power because its peak laser intensity was also the greatest.

However, output power alone does not tell the whole story. In this section, to obtain the time-integrated in-band flux density needed for CE calculation, we integrated both the input and output powers over the duration of the laser. Then, in taking the fraction of the former over the

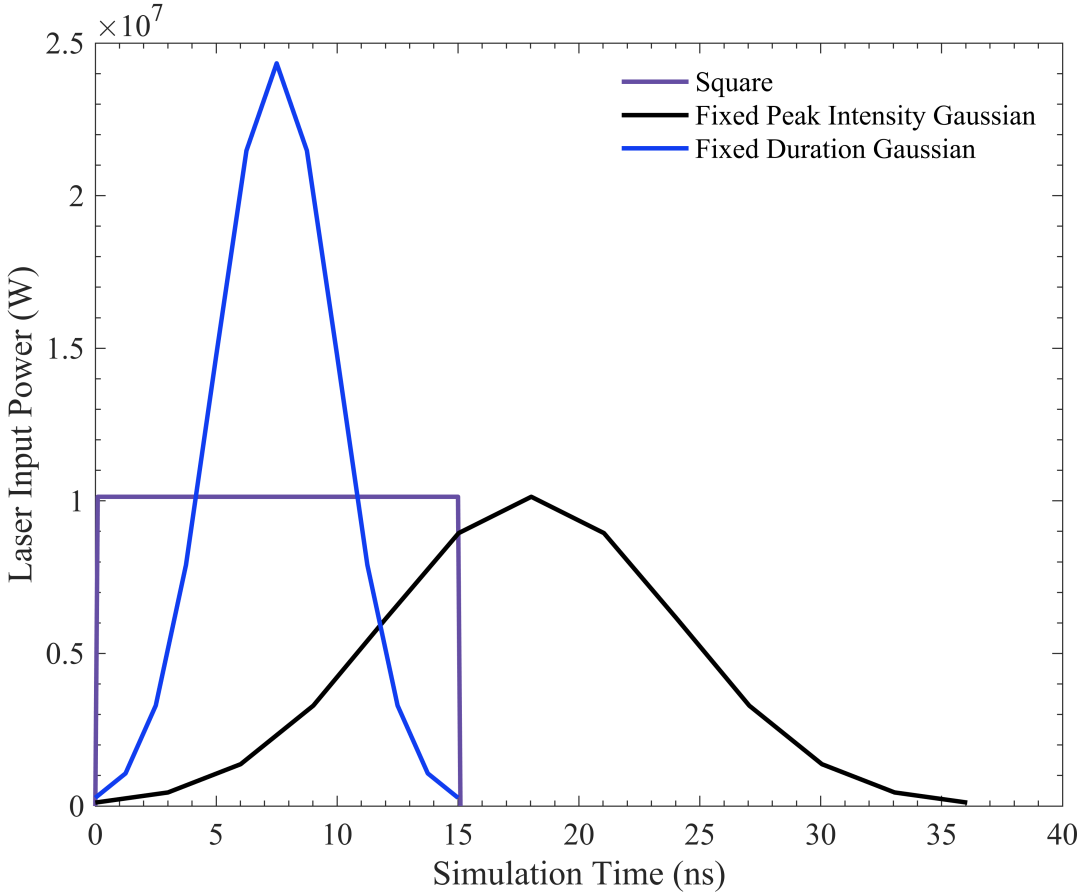

Figure 4.1: Pulse shape profiles of the three temporal profiles used in the constant energy pulse shape comparison — square , fixed peak intensity Gaussian, and fixed duration Gaussian.

latter to calculate the conversion efficiency, we found that the square pulse resulted in the highest conversion efficiency of the three profiles tested, with a CE of 2.24% compared to a CE of 2.04% for the fixed peak intensity Gaussian and 1.68% for the fixed duration Gaussian profiles. This finding — that the square pulse resulted in a higher CE than the Gaussian pulses — is in line with the primary finding in the previous pulse shaping study mentioned. [30]

Because the square pulse produced the highest CE of the three, its output profile, plotted in Figure 4.2(a), is worth analyzing in more detail. Interestingly, the output in-band power leveled off at its peak after 5 ns of lasing.at later times. This indicates that some time is needed

(a) Square Pulse (CE = 2.24%)

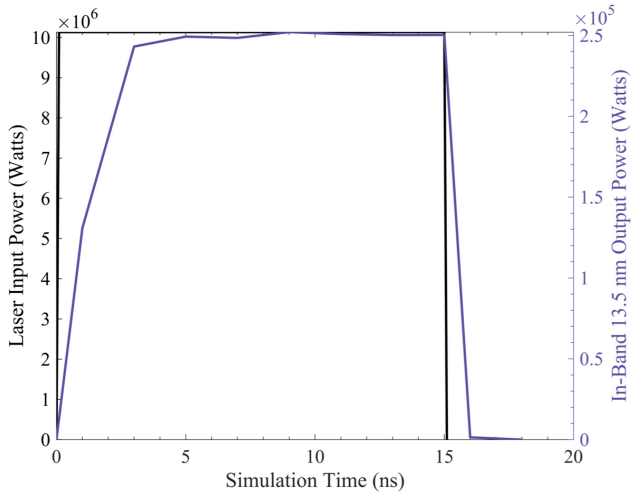

(b) Fixed Peak Intensity Gaussian (CE = 2.04%)

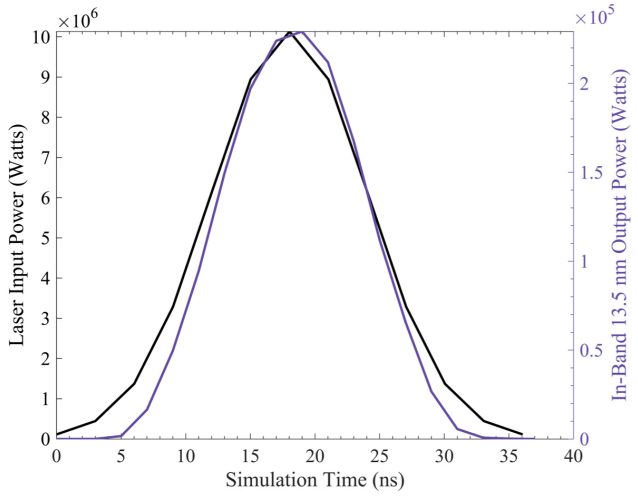

(c) Fixed Duration Gaussian (CE = 1.68%)

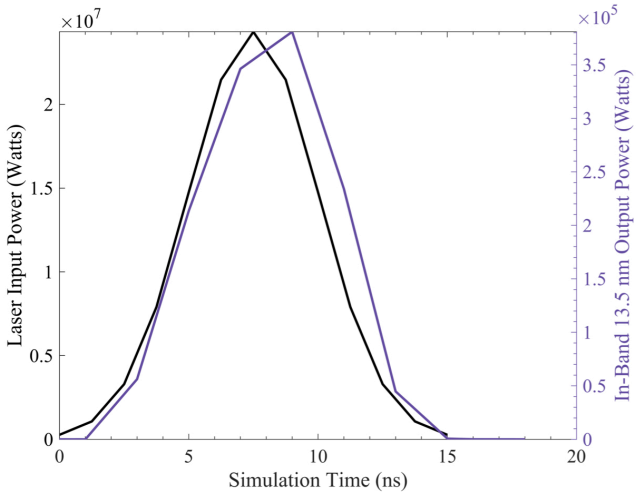

Figure 4.2: In-band light output over the course of the laser pulse duration overlaid over the input pulse shape for (a) square profile, (b) fixed peak intensity Gaussian profile, and (c) fixed duration Gaussian profile.

for the plasma to reach a steady state size of ideal temperature and density, making the initial portion of the square pulse low in efficiency. To improve upon the already high CE of the square pulse, a different pulse shape could be introduced in the first 5 ns to close the gap between the input and output power profiles — a concept we explored further in Section 4.4. Lastly, because the output laser continued at its peak throughout the duration of the pulse, and only dropped sharply after the laser was switched off, we conclude that the pulse duration used was insufficiently long, leaving some amount of output power (and, thus, CE) on the table. In fact, in increasing the pulse duration to 24 ns — the longest duration possible before FLASH encountered a negative 3T error for the setup used — we found that the conversion efficiency increases to 2.34%.

4.3 Novel Pulse Shape Profiles

On top of the three in the previous section, we explored an additional 5 different pulse shape profiles, all of which new to the EUV literature. The first set of pulses, what we call the "step down" pulses, came from the empirical idea that high EUV output could be maintained at a lower laser intensity, and thus lower input energy, after EUV output has leveled off. Building on on the observation that EUV output in the square pulse profile leveled off after 5 ns, an initially high intensity "pedestal" was used for the first 5 ns before the intensity was stepped down to a lower "foot".

As seen in Figure 4.3, we tested a total of three step down pulse combinations: (a) 1.4×10^{11} W/cm^2 stepped down to 1.0×10^{11} W/cm^2; (b) 1.4×10^{11} W/cm^2 stepped down to 1.2×10^{11} W/cm^2; and (c) 2.7×10^{11} W/cm^2 stepped down to 1.4×10^{11} W/cm^2, resulting in a conversion efficiency of 2.22%, 2.24%% and 1.87% respectively. While only the second pulse resulted in a

(a) Step Down 1.4 to 1.0×10¹¹ W/cm² (CE = 2.22%)

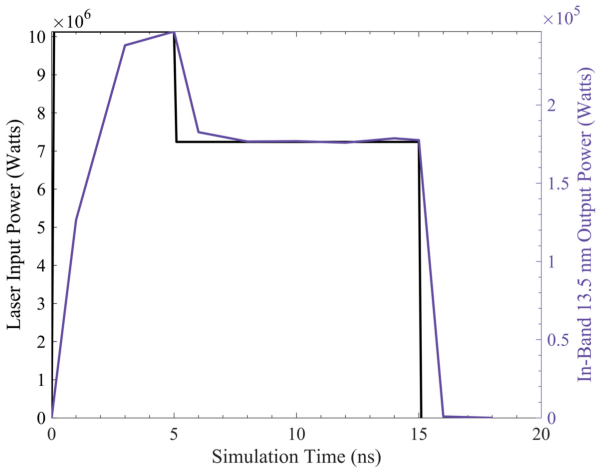

(b) Step Down 1.4 to 1.2×10¹¹ W/cm² (CE = 2.24%)

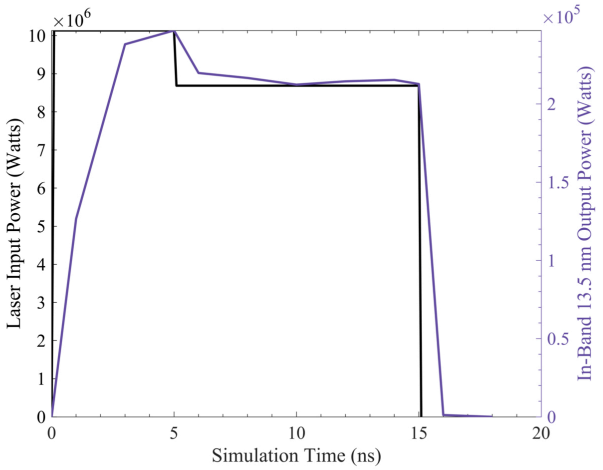

(c) Step Down 2.7 to 1.4×10¹¹ W/cm² (CE = 1.87%)

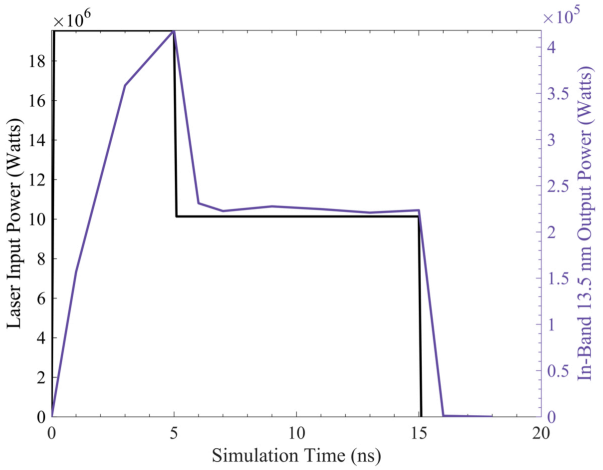

Figure 4.3: In-band light output over the course of the laser pulse duration overlaid over the input pulse shape for the "step down" pulse shapes. The pedestal duration used was fixed at 5 ns and the foot duration was fixed at 10 ns. Three intensity variations were used: (a) 1.4×10¹¹ W/cm² stepped down to 1.0×10¹¹ W/cm²; (b) 1.4×10¹¹ W/cm² stepped down to 1.2×10¹¹ W/cm²; and (c) 2.7×10¹¹ W/cm² stepped down to 1.4×10¹¹ W/cm².

CE close to the base square pulse case, it also used slightly less energy, making it an unequal comparison. A like-for-like comparison equalizing the energies between the two will be discussed further at the end of this section.

Next, we tested a set of "step up" pulses in which an initially low intensity "foot" was used to prepare the plasma for irradiation and then stepped up to the high intensity "pedestal". The idea for this pulse came from a similar pulse shape used in laser-driven inertial confinement fusion experiments, in which a low intensity foot, used to set the adiabat of the fusion target, is followed up with a ramp to compress the target and finished with a high intensity pedestal to launch shock compressions. [27] However, instead of using a ramp as in fusion, we opted for a stepwise increase instead as compression of the target was not the goal here.

With the step up pulse shape, we tested seven different foot intensities — 0.1%, 0.5%, 1%, 2.5%, 5%, 10% and 15% of the pedestal intensity — while keeping constant a 5 ns foot pulse duration, 1.4×10^{11} W/cm^2 pedestal intensity, and 15 ns pedestal pulse duration. The 0.1%, 0.5%, 1%, 2.5%, 5%, 10% and 15% intensities resulted in 2.29%, 2.33%, 2.33%, 2.31%, 2.28%, 2.26% and 2.24% conversion efficiencies respectively, with the 0.5% and 1% intensity cases achieving both the highest CEs of the step up pulses tested and higher CEs than the square pulse case tested in Section 4.3. The pulse shape profiles and their corresponding in band power outputs were plotted in Figure 4.4.

Then, to optimize for the foot durations, we tested three different foot durations — 3 ns, 5 ns, and 7 ns — with the peak CE, 1% foot intensity case, resulting in 2.32%, 2.33% and 2.33% conversion efficiencies respectively. These step up pulse shape profiles and their corresponding in-band power output were plotted as seen in Figure 4.5. This indicates that the 5 ns foot

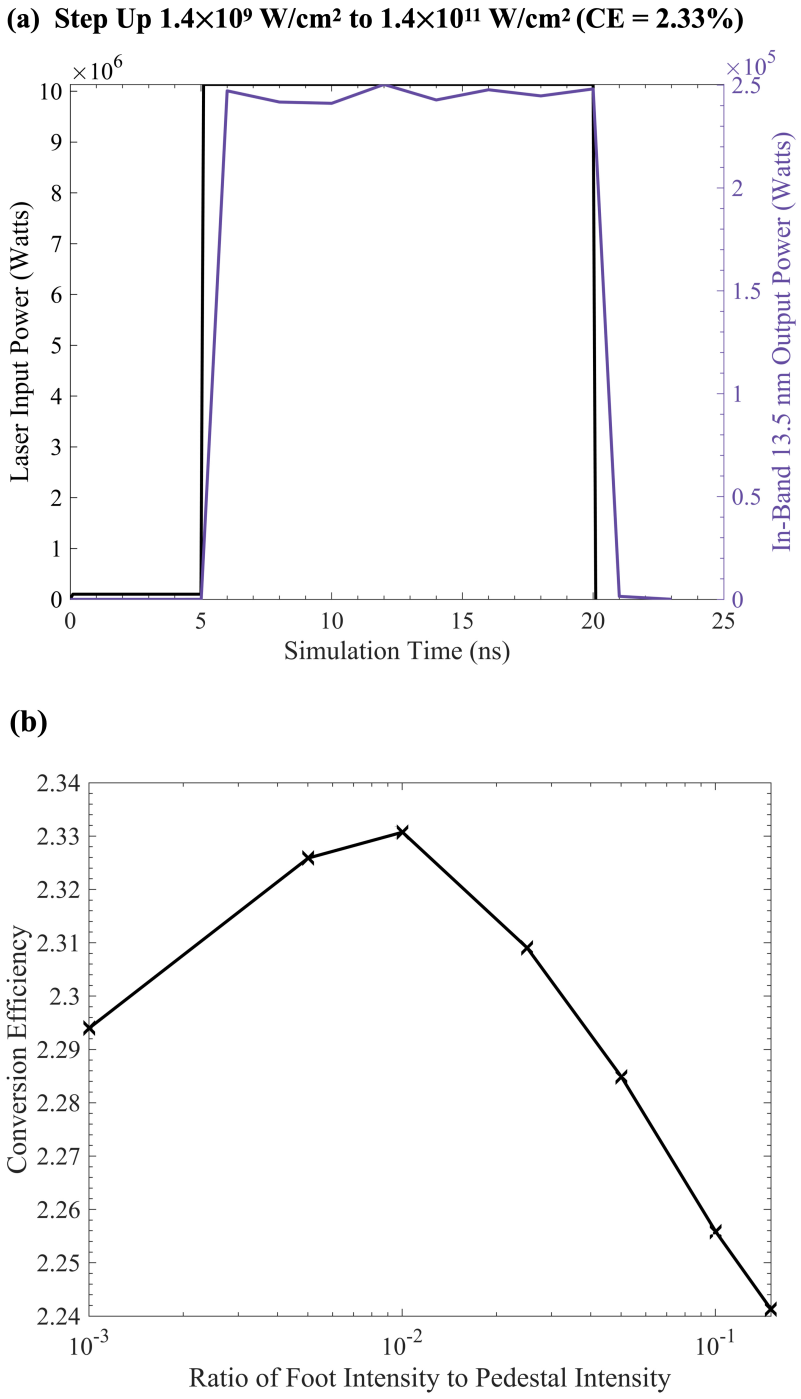

Figure 4.4: (a) In-band light output over the course of the laser pulse duration overlaid over the input pulse shape for a representative "step up" pulse shape — a foot intensity of 1%. The pedestal duration used was fixed at 15 ns, the foot duration was fixed at 5 ns, and the pedestal intensity was fixed at 1.4×10^{11} W/cm^2. (b) Plot of conversion efficiency vs the ratio of foot intensity used in the step up pulses tested.

(a) Step Up
3 ns Foot
(CE = 2.32%)

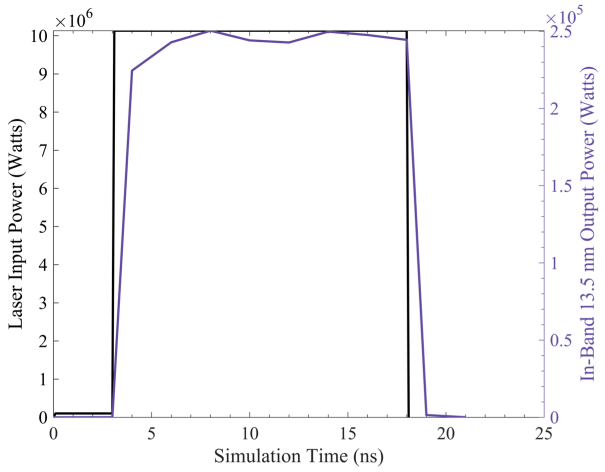

(b) Step Up
5 ns Foot
(CE = 2.33%)

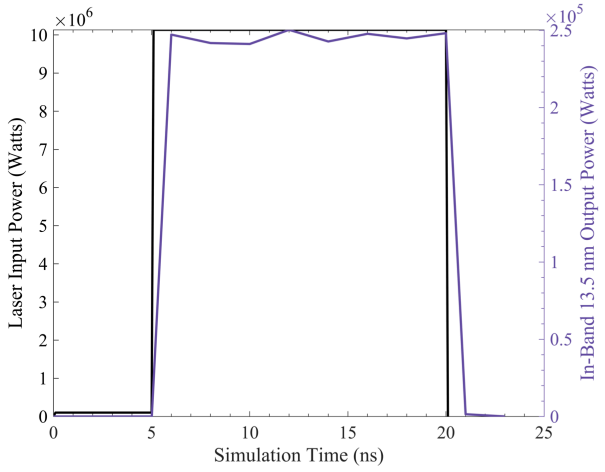

(c) Step Up
7ns Foot
(CE = 2.32%)

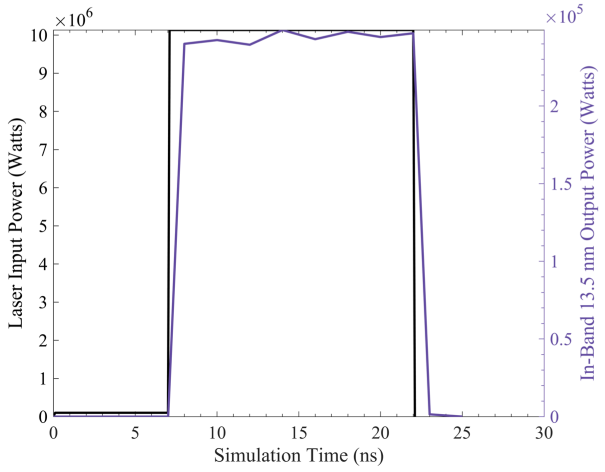

Figure 4.5: In-band light output over the course of the laser pulse duration overlaid over the input pulse shape for the "step up" pulse shape to measure the impact of foot duration on conversion efficiency. The pedestal duration was fixed at 15 ns, the pedestal intensity was fixed at 1.4×10^{11} W/cm^2, and the foot intensity was fixed at 1% of the pedestal intensity. Three foot duration variations were used: (a) 3 ns, (b) 5 ns, and (c) 7 ns.

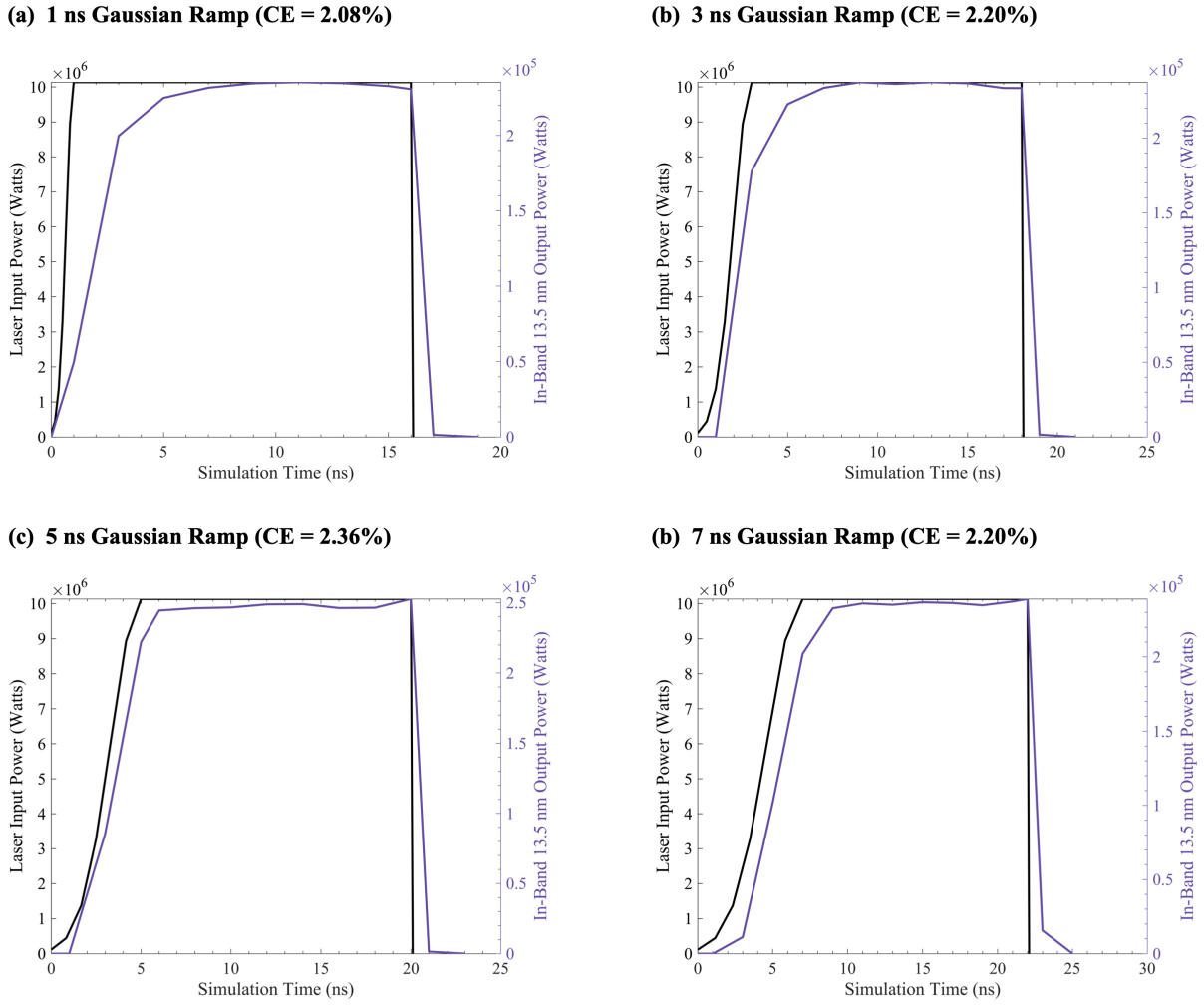

Figure 4.6: In-band light output over the course of the laser pulse duration overlaid over the input pulse shape for the "Gaussian ramp" pulse shape. The steady state duration was fixed at 15 ns and the peak intensity was fixed at 1.4×10^{11} W/cm^2. Four ramp duration variations were used: (a) 1 ns, (b) 3 ns, (c) 5 ns, and (d) 7 ns.

duration, 1% foot intensity case results in the highest CE of the step up pulse shapes tested.

The improvement of the step up pulse over the standard square pulse could be attributed to the minimization of laser energy reflection at the beginning of the pulse. When the tin target is initially irradiated by the laser, the process of inverse bremsstrahlung — the deposition of photon energy by electron-ion collisions — is inefficient as it requires a target density near the critical density of the 1 micron laser used. As such, instead of transferring the laser energy via inverse

Bremsstrahlung, a large amount of that initial laser energy is reflected from the surface of the target. Over time, the energy that does get absorbed by the target creates plasma with a lower and lower density, leading to more of the laser energy getting absorbed by the target. With the initial foot of the step up pulse, a much smaller amount of energy is used to create the critical density plasma, wasting a lower amount of energy to reflection than the high intensity square pulse.

The next set of pulses tested, the “Gaussian ramp” pulses, combines the close profile tracing of the Gaussian pulse and the high steady state EUV output of the square pulse by starting with a Gaussian ramp up and finishing with a square pulse shape. Similar to the step up pulse, the idea with the Gaussian ramp pulse was to gently ramp up the plasma to peak EUV output power and minimize the initial energy reflection. As seen in Figure 4.6, we tested a total of four ramp up durations, (a) 1 ns, (b) 3 ns, (c) 5 ns, (d) 7ns yielding conversion efficiencies of 2.08%, 2.20%, 2.20% and 2.16% respectively — all of which lower than that of the square pulse.

Lastly, a “mini prepulse” was tested with an initial 8.4 mJ prepulse . The 40 ns delay between prepulse and main pulse, shorter than the conventional delay of hundreds of nanoseconds to a couple microseconds in previous studies [32, 33], was chosen because the average electron density of the target and its surrounding plasma was found to decrease to the 1 micron critical density in that span of time, and thus would provide a critical surface for efficient inverse bremsstrahlung absorption. The pulse shape and its corresponding output was plotted in Figure 4.7 and the resulting conversion efficiency for the pulse is 1.5%. This low CE value could be attributed to the reduced confinement of plasma without a reduction in self absorption, resulting in a net decrease of in-band output energy generated. In the multi-microsecond delays

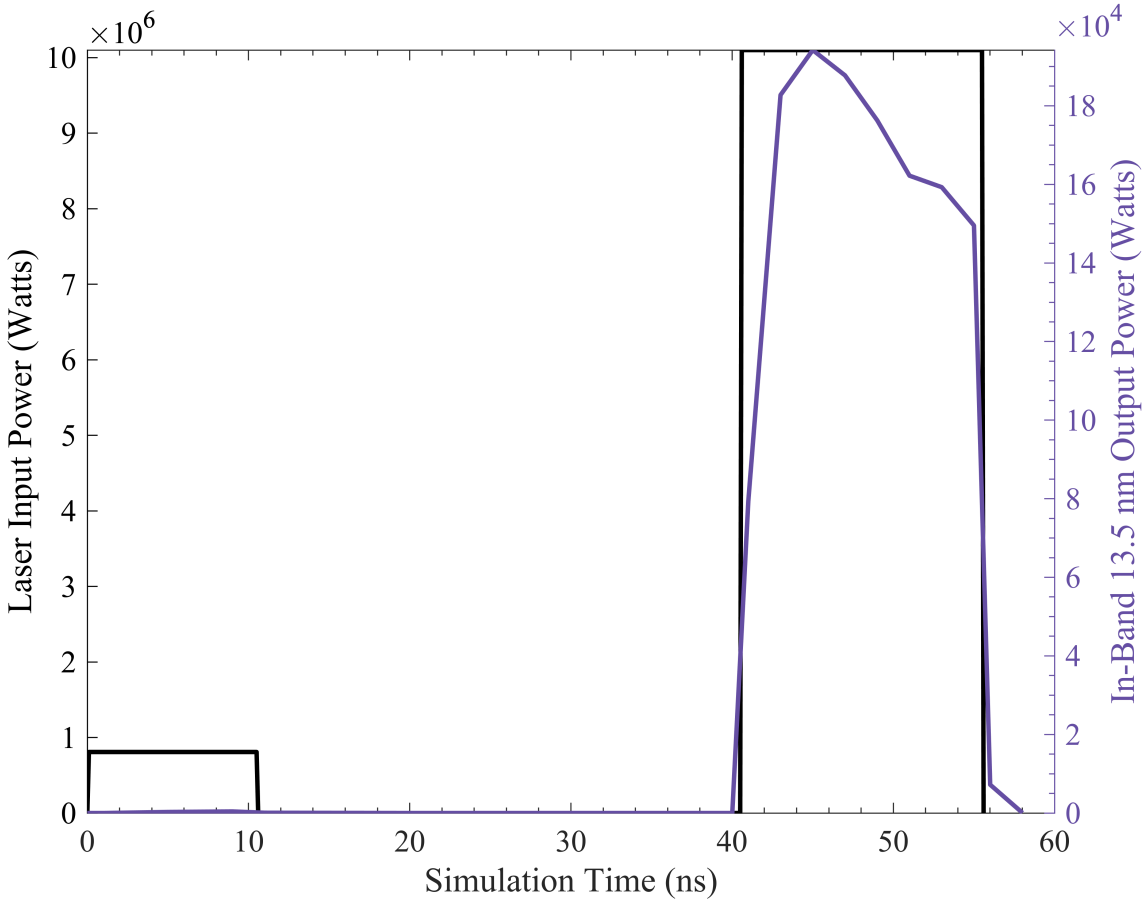

Figure 4.7: In-band light output over the course of the laser pulse duration overlaid over the input pulse shape for the "mini-prepulse" pulse shape. The prepulse energy was fixed at 8.4 mJ and prepulse duration was fixed at 10.6 ns. The main pulse used was a square pulse with pulse duration was fixed at 15 ns and peak intensity fixed at 1.4×10^{11} W/cm^2.

typically used, the plasma density is decreased to 10^{17} - 10^{18} cm^{-3} — lower than the density at which self-absorption of 13.5 nm light is significant.

While some of the novel pulses tested achieved a conversion efficiency higher than the 15 ns square pulse did, a direct comparison between those pulses and the square pulse is imperfect as they are not energy equivalent. Controlling for energy by comparing those pulses used with an interpolated square pulse of similar input energy, we found that three of the four pulses resulted in an improvement over the equivalent square pulses. Most notably, both the step

up pulse the Gaussian Ramp pulse resulted in approximately a 4% improvement in CE over the square pulse case, as seen in Table 4.1. This indicates that pulse shaping is a promising method to reduce laser energy reflection, and thus wastage, at the start of the pulse.

Table 4.1: Conversion efficiency comparisons between the best performing pulse shapes and their energy equivalent square pulses.

Pulse Shape	CE	CE of Energy Equivalent Square Pulse	Percentage Improvement over Square Pulse
Square Pulse	2.24%	2.24%	—
Step Down Pulse	2.24%	2.21%	1.4%
Step Up Pulse	2.33%	2.24%	4.0%
Gaussian Ramp Pulse	2.36%	2.27%	4.0%

4.4 Discussion

The conversion efficiencies obtained in study, whether on an absolute or relative scale, by no means represent the highest possible CEs of those individual pulse shapes. For instance, a longer pulse duration could result in a higher CE as evident from the sharp drop off at the end of lasing for the step up, step down and Gaussian ramp down. Additionally, a larger laser spot size for the Gaussian ramp and step up pulses might improve the confinement of the expanded plasma, and thus improve CE. Because a small improvement in conversion efficiency can result in a worthwhile improvement in wafers per hour — a 4% increase over the existing 125 wafers per hour corresponds to 5 more wafers made an hour — fine-tuning parameters for the highest conversion efficiency, however marginal the improvement, is worthwhile.

To achieve a greater level of accuracy and stronger confidence in the SPECT3D results, the simulations could be processed at a finer time step than the 1-to-2 ns steps we used in this study. With a time step of 0.5 ns and shorter, the greater output power detail captured could lead

to more insights into fine-tuning the pulse shapes. However, with the limited processing power available to us for use with SPECT3D, using such a short time step with the number of pulses tested would be too time-consuming, and as such was not attempted.

Lastly, the novel pulse shapes tested in Section 4.4, as well as the pulses tested in Reference 30, are by no means the be all end all of pulse shape innovation. Because of the pulse shape flexibility afforded by the new solid-state lasers, and with the promising results obtained in this study, there is ample room for more creativity in designing novel pulses. In addition to the application of basic plasma physics theory in informing new pulse shapes, machine learning, AI, and other statistical models could be used to further optimize the ideal pulse shape for EUV. In fact, a similar effort has proven successful in increasing the neutron yield for inertial confinement fusion. [34]

Chapter 4, in part, is currently being prepared for submission for publication of the material. Lee, Brian; Matsuo, Kazuki; Bailly-Grandvaux, Mathieu; Beg, Farhat. The thesis author was the primary investigator and author of this material.

Chapter 5. Conclusion and Future Work

5.1 Conclusion

In this study, we found that FLASH and SPECT3D in their default configurations were not able to perfectly replicate the spectra of an experimental 1-micron solid-state laser across different laser intensities. However, in addressing the main issues of the spectra — the higher effective laser intensity and left-shifted peaks — by reducing the simulation laser intensity and right-shifting the spectra, we found the new, adjusted spectra achieved a good level of modeling accuracy. Additionally, by testing a range of novel pulse shapes, we found that three of the four pulses tested — the "step down", "step up", and "Gaussian ramp" pulses resulted in 1.4%, 4.0% and 4.0% higher CEs than their equivalent-energy square pulse respectively, proving that pulse shapes beyond the standard square and Gaussian pulses have the potential to augment the efficiency of EUV sources.

In summary, FLASH and SPECT3D are two accessible simulation tools that, with some modifications, accurately model the single-pulse tin laser produced plasma process for EUV lithography. Additionally, by modifying the temporal pulse shape of the laser, higher conversion efficiencies than the standard square or Gaussian pulses are possible.

5.2 Future Work

Despite the successful benchmarking done in this study, more tests are needed to ensure that the FLASH-SPECT3D combination used here is robust across the parameter space. not just for a larger range of parameters but also for the parameters tested in this study. For instance, due to limitations in computational power, I was not able to verify the spectral accuracy of FLASH and SPECT3D for other laser spot sizes, laser pulse durations, and droplet sizes. Furthermore, with the promising results 2 micron lasers for other wavelengths of light like 2 micron. Aside from parameters outside the scope of this study, a retesting of the parameters tested in this study would also be helpful to further verify the results achieved here. Because of uncertainty in the experimental intensity, duration and spectra from Reference 13, in-house testing with the soon-to-come experimental facilities in UC San Diego would provide yet another set of data to verify the results — a luxury not afforded to us due to complications over the course of the pandemic.

More work is also necessary to enable accurate dual-pulse modeling in FLASH. In our brief testing of prepulse simulations on FLASH, we found that a low-energy prepulse completely evaporates the tin target instead of flattening it into a disk as observed experimentally. The time-evolution of the prepulse-irradiated tin droplet is displayed in Figure 5.1. In the figure, we see that the density drops dramatically between 40 ns and 50 ns, ruining the rest of the simulation after the 50 ns mark — instead of slight disk shape forming by 300 ns, a turbulent plasma at less than liquid density is left. This could be attributed to the model for surface tension, or the lack thereof, in FLASH. As such, in future studies, this should be taken into account, whether artificially by freezing the cells below a certain specified electron temperature or structurally by including surface tension equations into the code base.

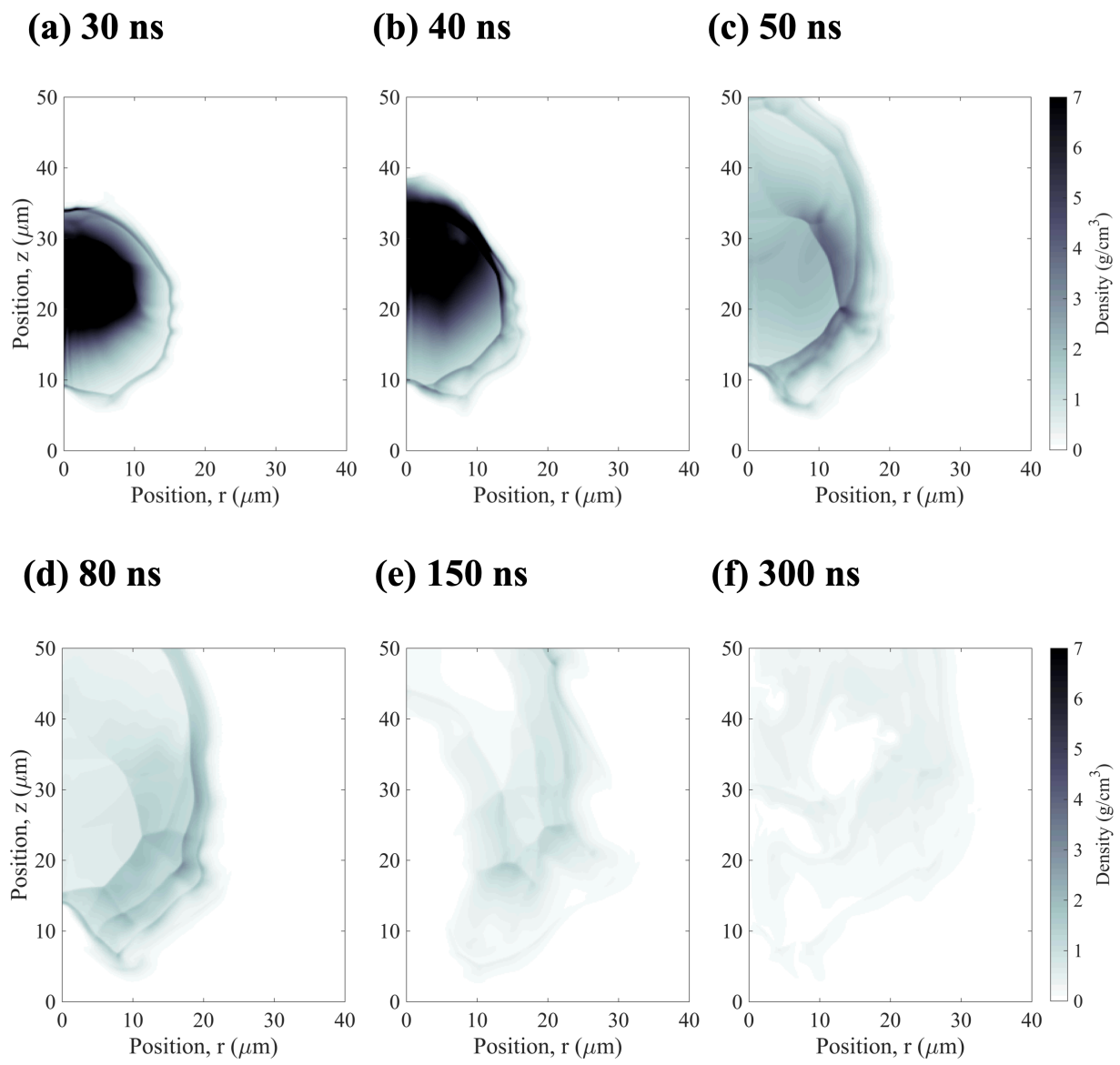

Figure 5.1: (a) - (f) Time evolution of an 8.4 mJ energy, 10.6 ns FWHM pulse duration prepulse-irradiated tin droplet. The tin droplet maintains solid-or-liquid density up to the 40 ns mark, after which the density drops rapidly, eventually completely evaporating by the 300 ns mark.

Lastly, building on the research into multiply-excited states in Reference 25, a method should be devised to incorporate that work into the FLASH and SPECT3D combo. Because the atomic model used in SPECT3D does not fully take into account the latest findings in tin multiply-excited states, a new atomic model should be built within the SPECT3D software

ecosystem to reflect the new research. One way this could be accomplished is through the AtomicModelBuilder application, in which the full range of atomic processes could be altered in their bundling and their relative rates.

Bibliography

[1] Waldrop, M. M. (2016). The chips are down for Moore's law. Nature, 530(7589), 144–147. https://doi.org/10.1038/530144a

[2] Owa, S., Wakamoto, S., Murayama, M., Yaegashi, H., Oyama, K. (2014) "Immersion lithography extension to sub-10nm nodes with multiple patterning," Proc. SPIE 9052, Optical Microlithography XXVII, 90520O; https://doi.org/10.1117/12.2046604

[3] Bakshi, V. (2018). Euv Lithography (SPIE Press Monographs) (2nd ed.). Society of Photo Optical.

[4] Rupp, K. (2018, February 15). 42 Years of Microprocessor Trend Data | Karl Rupp. Karl Rupp. https://www.karlrupp.net/2018/02/42-years-of-microprocessor-trend-data/

[5] Kelion, L. "Apple IPhone 12: The Chip Advance Set to Make Smartphones Smarter." BBC News, 13 Oct. 2020, www.bbc.com/news/technology-54510363.

[6] Lee, J. H., and Su-Bin. "Samsung to Ramp up EUV Scanners to Take on Foundry Leader TSMC." The Korea Economic Daily Global Edition, 15 Mar. 2021, www.kedglobal.com/newsView/ked202103150012.

[7] Bajt, S. Alameda J., Barbee T., Clift W., Folta J., Kaufmann B. and Spiller E. (2002). Improved reflectance and stability of Mo-Si multilayers. Optical Engineering, 41(8), 1797. https://doi.org/10.1117/1.1489426

[8] Nishihara, K., Sunahara, A., Sasaki, A., Nunami, M., Tanuma, H., Fujioka, S., Shimada, Y., Fujima, K., Furukawa, H., Kato, T., Koike, F., More, R., Murakami, M., Nishikawa, T., Zhakhovskii, V., Gamata, K., Takata, A., Ueda, H., Nishimura, H., Izawa, Y., Miyanaga, N., Mima, K. (2008). Plasma physics and radiation hydrodynamics in developing an extreme ultraviolet light source for lithography. Physics of Plasmas, 15(5), 056708. https://doi.org/10.1063/1.2907154

[9] Tanaka, H., Matsumoto, A., Akinaga, K., Takahashi, A., & Okada, T. (2005). Comparative study on emission characteristics of extreme ultraviolet radiation from CO2 and Nd:YAG laser-produced tin plasmas. Applied Physics Letters, 87(4), 041503. https://doi.org/10.1063/1.1989441

[10] Takahashi, A., Nakamura, D., Tamaru, K., Akiyama, T., & Okada, T. (2008). Comparative study on EUV and debris emission from CO2 and Nd:YAG laser-produced tin plasmas. Journal of Physics: Conference Series, 112(4), 042059. https://doi.org/10.1088/1742-6596/112/4/042059

[11] Hassanein, A., Sizyuk, V., Harilal, S. S., Sizyuk, T. (2020) ”Analysis, simulation, and experimental studies of YAG and CO2 laser-produced plasma for EUV lithography sources," Proc. SPIE 7636, Extreme Ultraviolet (EUV) Lithography, 76360A ; https://doi.org/10.1117/12.848222

[12] Fomenkov I. (2018). Int. Workshop on EUV and Soft X-Ray Sources https://euvlitho.com/2018/S1.pdf

[13] Schupp, R., Torretti, F., Meijer, R., Bayraktar, M., Scheers, J., Kurilovich, D., Bayerle, A., Eikema, K., Witte, S., Ubachs, W., Hoekstra, R., & Versolato, O. (2019). Efficient Generation of Extreme Ultraviolet Light From Nd:YAG-Driven Microdroplet-Tin Plasma. Physical Review Applied, 12(1). https://doi.org/10.1103/physrevapplied.12.014010

[14] Sistrunk, E., Alessi, D. A., Bayramian, A., Chesnut, K., Erlandson, A., Galvin, T. C., Gibson, D., Nguyen, H., Reagan, B., Schaffers, K., Siders, C. W., Spinka, T., and Haefner, C. (2019). “Laser Technology Development for High Peak Power Lasers Achieving Kilowatt Average Power and Beyond,” in *Short-pulse High-energy Lasers and Ultrafast Optical Technologies*, vol. 11034 (SPIE, 2019), pp. 1–8.

[15] Siders, C. W., Erlandson, A. C., Galvin, T. C., Frank, H., Langer, S., Reagan, B. A., Scott, H., Sistrunk, E. F., and Spinka, T. M. (2019)“Efficient high power laser drivers for next-generation High Power EUV sources,” in *2019 Source Workshop*, pp. 1–23.

[16] White, J., Dunne, P., Hayden, P., O’Reilly, F., & O’Sullivan, G. (2007). Optimizing 13.5nm laser-produced tin plasma emission as a function of laser wavelength. *Applied Physics Letters*, *90*(18), 181502. https://doi.org/10.1063/1.2735944

[17] Fujioka, S., Nishimura, H., Nishihara, K., Sasaki, A., Sunahara, A., Okuno, T., Ueda, N., Ando, T., Tao, Y., Shimada, Y., Hashimoto, K., Yamaura, M., Shigemori, K., Nakai, M., Nagai, K., Norimatsu, T., Nishikawa, T., Miyanaga, N., Izawa, Y., & Mima, K. (2005). Opacity Effect on Extreme Ultraviolet Radiation from Laser-Produced Tin Plasmas. Physical Review Letters, 95(23). https://doi.org/10.1103/physrevlett.95.235004

[18] Hassanein, A. (2009). Effects of plasma spatial profile on conversion efficiency of laser-produced plasma sources for EUV lithography. Journal of Micro/Nanolithography, MEMS, and MOEMS, 8(4), 041503. https://doi.org/10.1117/1.3224901

[19] Freeman, J. R., Harilal, S. S., Hassanein, A., & Rice, B. (2012). Effect of prepulse laser wavelength on EUV emission from CO2 reheated laser-produced Sn plasma. Applied Physics A, 110(4), 853–856. https://doi.org/10.1007/s00339-012-7164-3

[20] Hassanein, A., & Sizyuk, T. (2013). Laser produced plasma sources for nanolithography—Recent integrated simulation and benchmarking. Physics of Plasmas, 20(5), 053105. https://doi.org/10.1063/1.4807379

[21] Sizyuk, T., & Hassanein, A. (2020). Tuning laser wavelength and pulse duration to improve the conversion efficiency and performance of EUV sources for nanolithography. Physics of Plasmas, 27(10), 103507. https://doi.org/10.1063/5.0018576

[22] Michael A. Purvis, Alexander Schafgans, Daniel J. W. Brown, Igor Fomenkov, Rob Rafac, Josh Brown, Yezheng Tao, Slava Rokitski, Mathew Abraham, Mike Vargas, Spencer Rich, Ted Taylor, David Brandt, Alberto Pirati, Aaron Fisher, Howard Scott, Alice Koniges, David Eder, Scott Wilks, Anthony Link, Steven Langer, (2016). "Advancements in predictive plasma formation modeling," Proc. SPIE 9776, Extreme Ultraviolet (EUV) Lithography VII, 97760K; doi: 10.1117/12.2221991

[23] Basko, M. M. (2016). On the maximum conversion efficiency into the 13.5-nm extreme ultraviolet emission under a steady-state laser ablation of tin microspheres. Physics of Plasmas, 23(8), 083114. https://doi.org/10.1063/1.4960684

[24] Kulkarni, S., Golovkin, I., MacFarlane, J.(2014). EUV source modelling. Proceedings Volume 9048, Extreme Ultraviolet (EUV) Lithography V; 90481T. https://doi.org/10.1117/12.2044783

[25] Torretti, F., Sheil, J., Schupp, R., Basko, M. M., Bayraktar, M., Meijer, R. A., Witte, S., Ubachs, W., Hoekstra, R., Versolato, O. O., Neukirch, A. J., & Colgan, J. (2020b). Prominent radiative contributions from multiply-excited states in laser-produced tin plasma for nanolithography. Nature Communications, 11(1). https://doi.org/10.1038/s41467-020-15678-y

[26] *Flash Center for Computational Science*. (n.d.). FLASH Code. Retrieved July 27, 2021, from http://flash.uchicago.edu/site/flashcode/

[27] Fryxell, B., Olson, K., Ricker, P., Timmes, F. X., Zingale, M., Lamb, D. Q., MacNeice, P., Rosner, R., Truran, J. W., & Tufo, H. (2000). FLASH: An Adaptive Mesh Hydrodynamics Code for Modeling Astrophysical Thermonuclear Flashes. The Astrophysical Journal Supplement Series, 131(1), 273–334. https://doi.org/10.1086/317361

[28] Orban C., Fatenejad, M., Chawla, S., Wilks, S. C. & Lamb, D. Q. A Radiation-Hydrodynamics Code Comparison for Laser-Produced Plasmas: FLASH versus HYDRA and the Results of Validation Experiments, eprint arXiv:1306.1584 (2013)

[29] MacFarlane, J., Golovkin, I., Wang, P., Woodruff, P., & Pereyra, N. (2007). SPECT3D – A multi-dimensional collisional-radiative code for generating diagnostic signatures based on hydrodynamics and PIC simulation output. High Energy Density Physics, 3(1–2), 181–190. https://doi.org/10.1016/j.hedp.2007.02.016

[30] Yin, L., Wang, H., Reagan, B. A., Baumgarten, C., Lyu, Z., Soufli, R., Gullikson, E., Shlyaptsev, V. N., & Rocca, J. J. (2021). Using Temporally Synthesized Laser Pulses to Enhance the Conversion Efficiency of Sn Plasmas for EUV Lithography. IEEE Photonics Journal, 13(1), 1–15. https://doi.org/10.1109/jphot.2020.3047093

[31] Betti, R., Zhou, C. D., Anderson, K. S., Perkins, L. J., Theobald, W., & Solodov, A. A. (2007). Shock Ignition of Thermonuclear Fuel with High Areal Density. Physical Review Letters, 98(15). https://doi.org/10.1103/physrevlett.98.155001

[32] Fujioka, S., Shimomura, M., Shimada, Y., Maeda, S., Sakaguchi, H., Nakai, Y., Aota, T., Nishimura, H., Ozaki, N., Sunahara, A., Nishihara, K., Miyanaga, N., Izawa, Y., & Mima, K. (2008). Pure-tin microdroplets irradiated with double laser pulses for efficient and minimum-mass extreme-ultraviolet light source production. Applied Physics Letters, 92(24), 241502. https://doi.org/10.1063/1.2948874

[33] Schupp, R., Behnke, L., Bouza, Z., Mazzotta, Z., Mostafa, Y., Lassise, A., Poirier, L., Sheil, J., Bayraktar, M., Ubachs, W., Hoekstra, R., & Versolato, O. O. (2021). Characterization of angularly resolved EUV emission from 2-μm-wavelength laser-driven Sn plasmas using preformed liquid disk targets. Journal of Physics D: Applied Physics, 54(36), 365103. https://doi.org/10.1088/1361-6463/ac0b70

[34] Gopalaswamy, V., Betti, R., Knauer, J. P., Luciani, N., Patel, D., Woo, K. M., Bose, A., Igumenshchev, I. V., Campbell, E. M., Anderson, K. S., Bauer, K. A., Bonino, M. J., Cao, D., Christopherson, A. R., Collins, G. W., Collins, T. J. B., Davies, J. R., Delettrez, J. A., Edgell, D. H., Epstein, R., Forrest, C. J., Froula, D. H., Glebov, V. Y., Goncharov, V. N., Harding, D. R., Hu, S. X., Jacobs-Perkins, D. W., Janezic, R. T., Kelly, J. H., Mannion, O. M., Maximov, A., Marshall, F. J., Michel, D. T., Miller, S., Morse, S. F. B., Palastro, J., Peebles, J., Radha, P. B., Regan, S. P., Sampat, S., Sangster, T. C., Sefkow, A. B., Seka, W., Shah, R. C., Shmyada, W. T., Shvydky, A., Stoeckl, C., Solodov, A. A., Theobald, W., Zuegel, J. D., Gatu Johnson, M., Petrasso, R. D., Li, C. K., Frenje, J. A. (2019). Tripled yield in direct-drive laser fusion through statistical modelling. Nature, 565(7741), 581–586. https://doi.org/10.1038/s41586-019-0877-0